PSR Report 2629

MAGNETIC SIGNATURES OF SUBMARINES II

P. M. Moser

February 1996

Phase Report
Contract N62269-94-C-1208

Sponsored by

Naval Air Warfare Center
Aircraft Division Warminster
Warminster, PA 18974

PACIFIC-SIERRA RESEARCH CORPORATION
600 Louis Dr., Suite 103 • Warminster, PA 18974 • (215) 441-4461, FAX (215) 441-0868
2901 28th Street • Santa Monica, CA 90405 • (310) 314-2300, FAX (310) 314-2323

REPORT DOCUMENTATION PAGE

Form Approved
OMB No. 0704-0188

1. REPORT DATE *(DD-MM-YYYY)*	2. REPORT TYPE	3. DATES COVERED *(From - To)*
xx-02-1996	Final technical	To February 1996

4. TITLE AND SUBTITLE
Magnetic Signatures of Submarines II

5a. CONTRACT NUMBER
N62269-94-C-1208

5b. GRANT NUMBER

5c. PROGRAM ELEMENT NUMBER

6. AUTHOR(S)
Moser, Paul M.

5d. PROJECT NUMBER

5e. TASK NUMBER

5f. WORK UNIT NUMBER

7. PERFORMING ORGANIZATION NAME(S) AND ADDRESS(ES)
Pacific-Sierra Research Corporation
Warminster, PA 18974

8. PERFORMING ORGANIZATION REPORT NUMBER
PSR Report 2629

9. SPONSORING/MONITORING AGENCY NAME(S) AND ADDRESS(ES)
Naval Air Warfare Center Aircraft Division Warminster
Warminster, PA 18974

10. SPONSOR/MONITOR'S ACRONYM(S)
NAWCADWAR

11. SPONSOR/MONITOR'S REPORT NUMBER(S)

12. DISTRIBUTION/AVAILABILITY STATEMENT
Approved for public release, distribution unlimited

13. SUPPLEMENTARY NOTES
See also PSR Report 2474, "Magnetic Signatures of Submarines I" by the same author.

14. ABSTRACT
This report covers a continuation of work described in PSR Report 2474. In the earlier study it became apparent that a great portion of the variability of the magnetic anomaly signatures stemmed not from the submarine-centered anomaly itself but rather from the path of the airborne magnetometer through the anomaly. Accordingly, this study focused on the anomaly in target-fixed coordinates, revealing the lobe structure of the anomaly, which, in turn, enabled a clearer understanding of the signatures produced by an airborne magnetometer. Additionally, temporal and spatial dependencies of magnetic anomalies from modulated galvanic currents were determined in both target-fixed and sensor-fixed coordinates.

15. SUBJECT TERMS
Submarine, Detection, Magnetic, Signature, Anomaly, Aircraft, Magnetometer, Model, Dipole, Antisubmarine Warfare, Nonacoustic Detection of Submarines

16. SECURITY CLASSIFICATION OF:			17. LIMITATION OF ABSTRACT	18. NUMBER OF PAGES	19a. NAME OF RESPONSIBLE PERSON
a. REPORT	b. ABSTRACT	c. THIS PAGE			19b. TELEPHONE NUMBER *(Include area code)*
unclassified	unclassified	unclassified	unlimited	69	

CONTENTS

FIGURES

FIGURES (continued)

FIGURES (continued)

I. INTRODUCTION

A submarine can cause a local distortion of the earth's naturally occurring magnetic field and thereby produce a *magnetic anomaly.* Submarine-generated magnetic effects arise from the *permanent* and *induced* magnetization of the ferromagnetic material constituting the structure and machinery of the submarine and from galvanic corrosion currents flowing through the submarine and the surrounding water.

Permanent magnetization results from the long-term alignment of the submarine with the earth's magnetic field and is enhanced if the hull is stressed through vibration, mechanical shock or submergence and subsequent relaxation. Over short time periods, the permanent magnetization is independent of the submarine's heading.

Even if the submarine is not permanently magnetized, it can still produce a local distortion of the fairly uniform magnetic field of the earth. This distortion can be described as if it originates from a temporary, orientation-dependent, induced magnetization of the submarine.

Electric currents produce magnetic fields. Galvanic corrosion currents arise from differences in electric potential of interconnected dissimilar metals immersed in an electrolytic solution such as a bronze propeller in electrical contact with a steel hull protected against corrosion by attached sacrificial zinc blocks, all immersed in sea water. The potential difference between the propeller and the zincs is about 1 volt and the resulting current may range from 1 to 100 amperes. Because of variations in resistance (as a function of propeller shaft angle) between the rotating propeller shaft and its bearings, this current may be modulated at the shaft rate. Thus a submarine may be surrounded by steady and alternating fields resulting from corrosion currents.

Each of the foregoing contributes to the submarine's magnetic signature, which represents a potentially rich source of ASW-relevant information. An understanding of such signatures should contribute to the optimum processing of signals which may yield improved target acquisition range, improved search strategy, target classification, and heading and depth information.

This present report is a continuation of work described in reference (a). In reference (a), equations were developed for describing the magnetic anomaly of a submarine as it would appear to an airborne scalar total-field magnetometer passing through it at constant velocity. In this earlier study, the submarine was treated as both a point ferromagnetic dipole and as an extended ferromagnetic dipole possessing both induced and permanent magnetic moments. In addition, expressions for the magnetic anomaly from the steady galvanic corrosion current (but not from the alternating component) and the combination of all of the above were derived as observable by an airborne sensor. In the earlier study it became apparent that a great portion of the variability of the signatures stemmed from not the target-centered anomaly itself but rather from the path that the sensor took through the anomaly. Therefore, it was decided

in the present study to calculate the anomaly in target-fixed coordinates. This approach revealed the lobe structure of the anomaly which, in turn, enabled a clearer understanding of the signatures that an airborne magnetometer produces. In addition, in the present study, the temporal and spatial dependencies of the magnetic anomaly from modulated (alternating) galvanic currents were determined and are presented here in both target-fixed and sensor-fixed coordinates.

II. FERROMAGNETIC ANOMALY OF A SUBMARINE

Ferromagnetic Moment of a Submarine

The *magnetic source strength* of a submarine is described in terms of its *magnetic moment*, which is a vector quantity whose magnitude and direction depend principally upon the magnitude and direction of the local magnetic field of the earth, the mass and shape of ferromagnetic material constituting the submarine, and the orientation of the submarine in the earth's field.

In reference (b), Peizer has provided simple formulas for calculating the induced and equilibrium magnetic dipole moments based on the shape and volume enclosed within a steel prolate spheroid approximation of a submarine. These formulas were generalized somewhat and recast in reference (a) as follows:

$$M_{VE} = -V\, H_V\, T \tag{1}$$

$$M_L = M_{LI} + M_{LP} = L\, H_L\, T + M_{LP} = L\, H_H\, T \cos(\beta - \alpha) + M_{LP} \tag{2}$$

$$M_A = M_{AI} + M_{AP} = A\, H_A\, T + M_{AP} = A\, H_H\, T \sin(\beta - \alpha) + M_{AP} \tag{3}$$

in which

M_{VE} = equilibrium vertical ferromagnetic moment ($\gamma \cdot ft^3$)
M_L = longitudinal component of ferromagnetic moment ($\gamma \cdot ft^3$)
M_{LI} = induced longitudinal moment ($\gamma \cdot ft^3$)
M_{LP} = permanent longitudinal moment ($\gamma \cdot ft^3$)
M_A = athwartship component of ferromagnetic moment ($\gamma \cdot ft^3$)
M_{AI} = induced athwartship moment ($\gamma \cdot ft^3$)
M_{AP} = permanent athwartship moment ($\gamma \cdot ft^3$)
V = coefficient for equilibrium vertical component of moment (ft^3/ton)
L = coefficient for induced longitudinal component of moment (ft^3/ton)
A = coefficient for induced athwartship component of moment (ft^3/ton)
H_V = vertical component of the earth's field (γ)
H_L = longitudinal component of the earth's field (γ)
H_A = athwartship component of the earth's field (γ)
H_H = horizontal component of the earth's field (γ)
T = submerged displacement of the submarine (tons)
α = submarine heading (degrees true)
β = local geomagnetic declination (degrees; east, positive).

Figure 1 illustrates the magnetization of a submarine in the earth's magnetic field and the corresponding vector components of the submarine's magnetic moment.

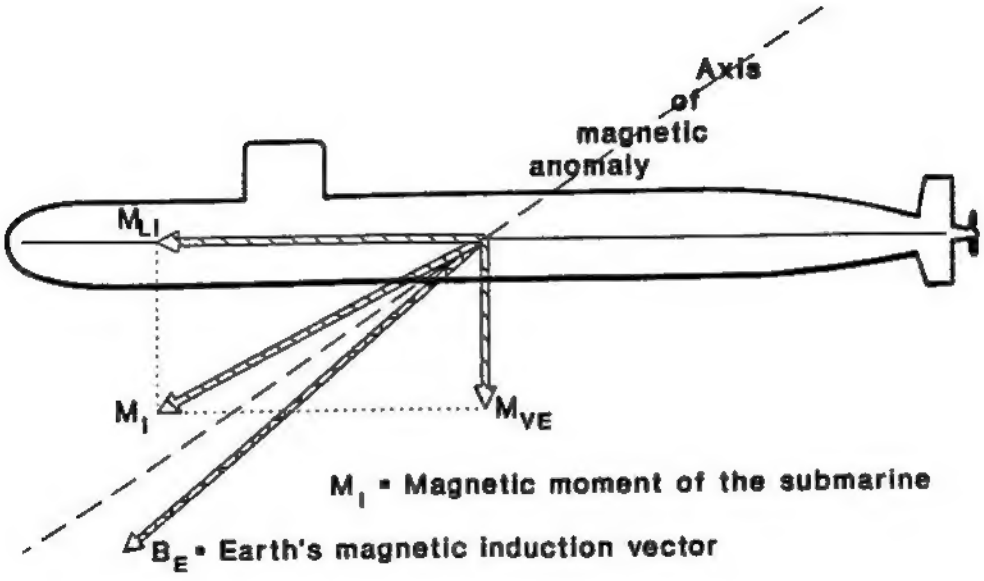

Figure 1. Magnetization of a submarine in the earth's magnetic field.

In equations (1), (2), and (3) the positive directions of M_{VE}, M_L, and M_A are vertically upward, stern-to-bow, and portside-to-starboard, respectively. The positive direction of H_V is, consistent with convention, vertically downward. The magnitude of the resultant moment is

$$M = (M_{VE}^2 + M_L^2 + M_A^2)^{1/2}. \quad (4)$$

Peizer provides values for the coefficients of magnetic moments for six classes of submarines. He gives a single value of V = 5.1 ft^3/ton for all six classes but six values for L ranging from 10.6 to 16.6 ft^3/ton and a calculated value of L = 11.5 ft^3/ton. He gives three values for A (2.9, 2.9, and 3.6 ft^3/ton) and a suggested value of A = 3.0 ft^3/ton.

Magnetic Induction from a Point Ferromagnetic Dipole

At distances that are large in comparison with the length of a submarine, its magnetic field may be assumed to originate from a point magnetic dipole centered at the submarine. The vector field **B** produced by a point magnetic dipole is given by

$$\mathbf{B} = -\mathbf{M}/R^3 + (3\,\mathbf{M}\cdot\mathbf{R})\,\mathbf{R}/R^5. \quad (5)$$

In equation (5) and the following equations, bold type indicates vector quantities. **R** is the radius vector from the dipole to the field point P at which the magnetic field is to be calculated, R is the magnitude of **R**, **B** is the magnetic induction vector at P, and **M** is the magnetic moment vector of the dipole. An inspection of equation (5) shows that, at a given

distance R, the magnitude B is twice as great along the dipole axis (for which $\mathbf{M}\cdot\mathbf{R} = MR$) as along the perpendicular bisector of the dipole (for which $\mathbf{M}\cdot\mathbf{R} = 0$).

For some purposes, it is useful to rewrite equation (5) in scalar form as

$$B_D = (3\cos^2\theta + 1)^{1/2} M/R^3 \tag{6}$$

in which B_D is the magnitude of the magnetic induction from the ferromagnetic dipole and θ is the angle between the positive dipole axis and the direction to P. In equation (6) it is more readily apparent that, at any given orientation, the magnetic induction is directly proportional to the magnetic moment and it varies inversely as the cube of the distance from the dipole. It should be observed that, along the dipole axis (i.e., for $\theta = 0°$), equation (6) reduces to $B_D = 2\ M/R^3$ whereas, perpendicular to the dipole axis (i.e., for $\theta = 90°$), $B_D = M/R^3$.

If θ_M is the angle of the dipole axis relative to a coordinate system whose origin is at the dipole and θ_R is the angle of a line from the origin to field point P, then $\theta = \theta_R - \theta_M$. If equation (6) is solved for R, one obtains the range R_B, as a function of angle, for which the magnetic induction from the ferromagnetic dipole has the magnitude B_D, i.e.,

$$R_B = \{[3\cos^2(\theta_R - \theta_M) + 1]^{1/2} M/B_D\}^{1/3}. \tag{7}$$

In figure 2, equation (7) is plotted in two dimensions for $M = 1.55 \times 10^9\ \gamma \cdot ft^3$ and $B_D = 0.03\ \gamma$. This figure may be thought of as a vertical slice through a three-dimensional shape that would result from rotating the curve about the dipole axis.

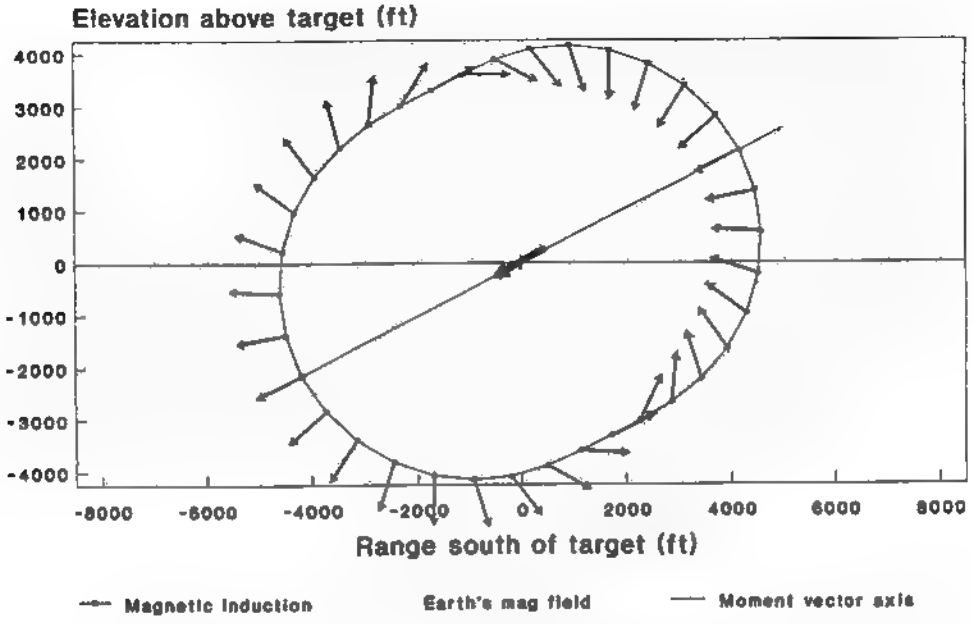

Figure 2. Vertical section of the locus of points for which magnetic induction from a point ferromagnetic dipole of moment $1.55 \times 10^9\ \gamma \cdot ft^3$ has a constant value $B_D = 0.03\ \gamma$.

A more complete representation of the magnetic induction from the dipole must also take into account the direction θ_B of the **B** vector at each point P. It can be shown that

$$\theta_B = \theta_R + \arctan[0.5 \sin(\theta_R - \theta_M) / \cos(\theta_R - \theta_M)]. \quad (8)$$

Figure 2 shows 36 vectors, all of magnitude $B_D = 0.03\ \gamma$, at orientation angles θ_B given by equation (8). The array of parallel dotted lines in figure 2 represents the direction of the earth's magnetic field.

Magnetic Anomaly from a Point Ferromagnetic Dipole

Scalar magnetometers, such as those commonly used for air ASW, measure the magnitude of the vector sum of the magnetic induction vectors of the earth and of the submarine. The magnetic induction of the earth is typically thousands of times greater than of the submarine at ranges of interest; thus the magnetic signature of the submarine represents only a tiny perturbation in the observed field. The large background field of the earth is usually removed by scalar subtraction and/or filtering; the residue is the submarine's *magnetic anomaly*. In Appendix A, equation (5) is expanded and equations are given for calculating the magnetic induction components and the magnetic anomaly in the earth's field at any point P.

It is shown in Appendix H of reference (a) that the magnetic anomaly of a submarine is given, to an excellent approximation, as simply the magnitude of the component of the submarine's magnetic induction vector in the direction of the earth's magnetic induction vector. If the vectors drawn in figure 2 are examined, it is seen that, in the upper right and lower left portions of the figure, they are aligned parallel to the downward-directed earth's field lines and therefore, at those two locations, add in a maximum positive sense to the earth's field. On the other hand, at two locations lying along the perpendicular to that direction, the vectors are anti-parallel to the direction of the earth's field and therefore add to it in a maximum negative sense. Thus, the anomaly exhibits two positive and two negative maximum absolute values. In addition, there are four intermediate angular positions at which the magnetic induction vectors from the submarine are perpendicular to those of the earth; nulls (of the magnetic anomaly) occur at these locations because the components of these vectors in the direction of the earth's field are zero.

Figure 3 shows, in submarine-fixed coordinates, a vertical slice through the anomaly inscribed within the magnetic induction curve. One could obtain the anomaly curve of figure 3 by calculating and plotting the projections of the vectors along the earth's field lines at each point of the curve of figure 2. Figure 3 represents the locus of points in a vertical plane for which the magnetic anomaly is $0.03\ \gamma$. The two larger lobes correspond to positive portions of the anomaly and the two smaller ones to negative portions.

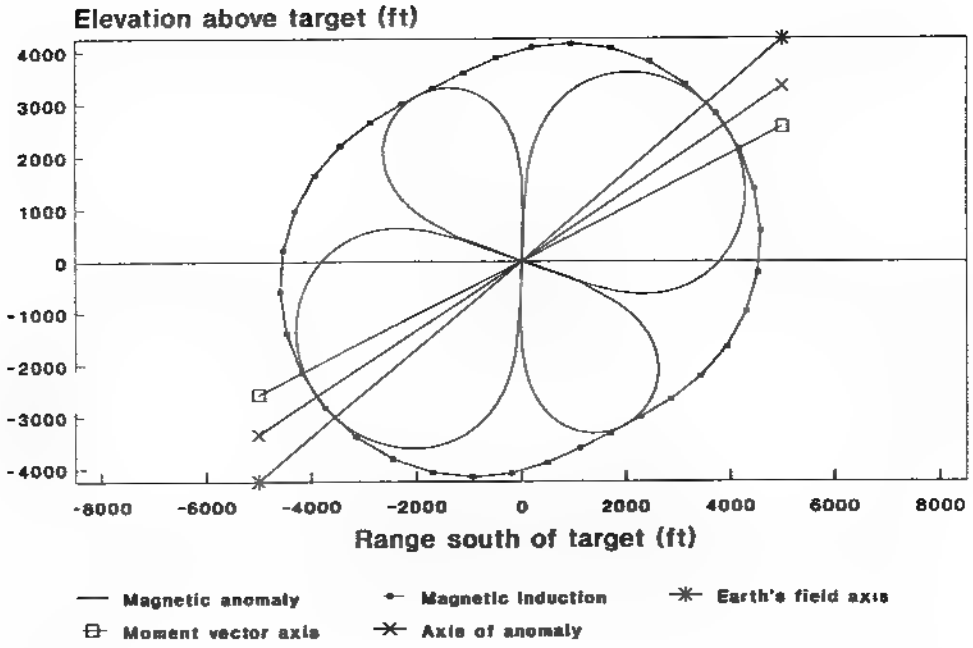

Figure 3. Vertical section of magnetic anomaly from a point ferromagnetic dipole.

The need for vector addition can be avoided by use of the following scalar approach. Let θ_E be the direction of the earth's field and, as before, let θ_M be the direction of vector **M**, and θ_R the direction of vector **R**. The magnetic anomaly Γ as a function of angle θ_R can be obtained by regarding the two terms on the right side of equation (5) as separate vectors, the first in the direction of **M** and the second in the direction of **R**. By multiplying the cosines of the angles between these vectors and the earth's field vectors (i.e. $\cos(\theta_M-\theta_E)$ and $\cos(\theta_R-\theta_E)$, respectively) one determines their components in the direction of the earth's magnetic field. These components are then added algebraically. Thus

$$\Gamma = -(M/R^3)\cos(\theta_M-\theta_E) + 3\,M/R^3\cos(\theta_R-\theta_M)\cos(\theta_R-\theta_E). \tag{9}$$

It follows that the locus of ranges R_Γ as a function of θ_R for any given positive or negative value of Γ is given by

$$R_\Gamma{}^3 = [3\cos(\theta_R-\theta_M)\cos(\theta_R-\theta_E) - \cos(\theta_M-\theta_E)]\,M/\Gamma. \tag{10}$$

The factor $\cos(\theta_R-\theta_M)$ arises from the scalar product $\mathbf{M}\cdot\mathbf{R}$ in equation (5).

Actually, equation (10) was used to plot the anomaly curve shown in figure 3. [Note: It was necessary to insert both positive and negative values of Γ into equation (10) to obtain both the positive and negative lobes of the anomaly. However, only the non-negative values of R^3 that resulted were selected and their cube roots taken to determine R as a function of θ_R.]

The angular positions of the maximum values of R_Γ can be determined from equation (10) by taking the first derivative of $R_\Gamma{}^3$ with respect to θ_R, setting it equal to zero, and solving for θ_R. Thus

$$\cos(\theta_R-\theta_M)\,[-\sin(\theta_R-\theta_E)] + \cos(\theta_R-\theta_E)\,[-\sin(\theta_R-\theta_M)] = 0. \tag{11}$$

Equation (11) can be rewritten as the sine of the sum of the two angles $(\theta_R-\theta_E)$ and $(\theta_R-\theta_M)$. Thus

$$\sin[(\theta_R-\theta_E) + (\theta_R-\theta_M)] = \sin(2\,\theta_R - \theta_E - \theta_M) = 0. \tag{12}$$

Equation (12) is satisfied if $(2\,\theta_R - \theta_E - \theta_M) = n\,\pi$ radians, in which n = 0, 1, 2, 3. Therefore, maxima occur at angles

$$\theta_R = (\theta_E + \theta_M + n\,\pi)/2. \tag{13}$$

For n = 0, it is seen that $\theta_R = (\theta_E + \theta_M)/2$. That is, the angle at which the first maximum of the anomaly occurs is simply the average of the angles of the earth's field vector and the submarine's magnetic moment vector. In other words, the axis of the anomaly bisects the angle between these two vectors as shown in figure 3. Other maxima occur and are equally spaced at angular separations of $\pi/2$ radians or 90°.

The value of $R_\Gamma{}^3$ at the first maximum can be obtained by inserting $\theta_R = (\theta_E + \theta_M)/2$ into equation (10). Thus

$$R_\Gamma{}^3{}_{max1} = \{3\cos^2[(\theta_E-\theta_M)/2] - \cos(\theta_E-\theta_M)\}\,M/\Gamma. \tag{14}$$

Similarly, the value of R^3 at the second maximum can be obtained by inserting $\theta_R = (\theta_E + \theta_M + \pi)/2$ into equation (13). Thus

$$R_\Gamma{}^3{}_{max2} = \{3\sin^2[(\theta_E-\theta_M)/2] + \cos(\theta_E-\theta_M)\}\,M/(-\Gamma). \tag{15}$$

The negative sign in equation (15) implies a negative value must be inserted for Γ.

By symmetry, the third and fourth maxima are equivalent to the first and second maxima, respectively.

If the angle ($\theta_E - \theta_M$) between the earth's magnetic field vector and the submarine's ferromagnetic dipole moment vector is small, equation (14) reduces to $R_\Gamma{}^3{}_{max1} \approx 2\,M/\Gamma$ and equation (15) reduces to $R_\Gamma{}^3{}_{max2} \approx M/(-\Gamma)$. Thus, subject to this assumption, the absolute values of the anomaly at its maxima are equal to the values of B_D at the same angular positions.

If the anomaly curve of figure 3 were to be rotated about the indicated axis of the anomaly, a three-dimensional representation of the ferromagnetic anomaly which may surround a submarine would result having the appearance of figure 4.[1] It consists of two parts: a doughnut-shaped ring or toroid and what appears to be a dumbbell or a partially inflated balloon that has been shoved halfway through the hole of the toroid. These curved surfaces are the locus of points for which the magnetic induction is 0.03 γ greater than or less than the ambient field of the earth. The value on the toroid surface is negative relative to the earth's field and that on the dumbbell surface is positive.

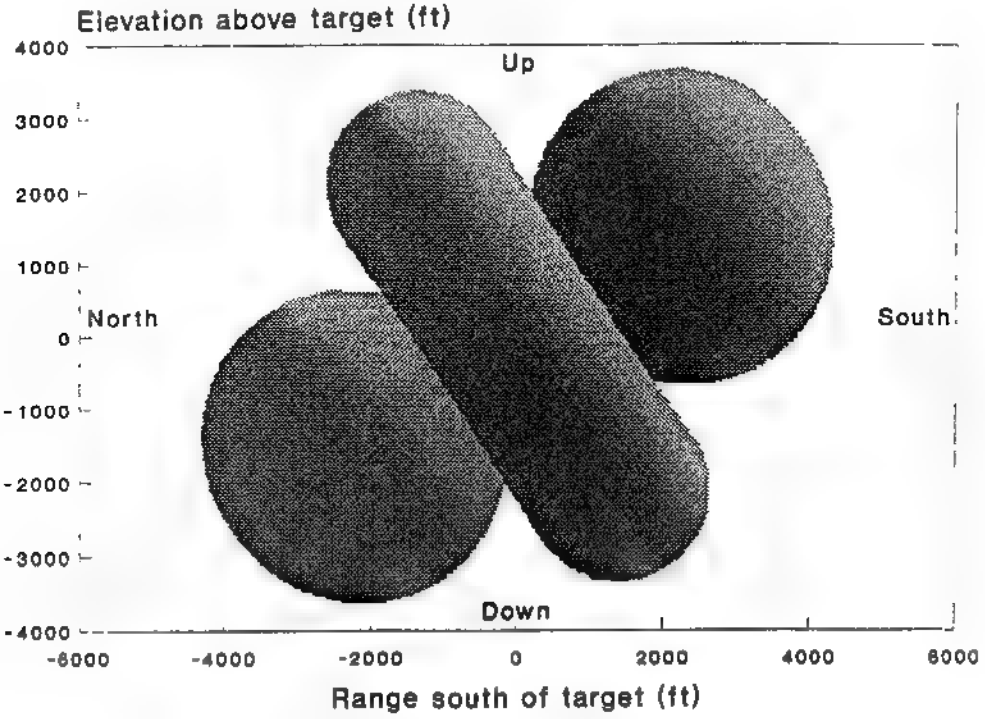

Figure 4. Three-dimensional plot of the anomaly from a point ferromagnetic dipole.

Figure 5 illustrates a single vertical slice through the anomaly of figure 4. In addition, it shows contours for +/–0.003 γ, +/–0.3 γ, and +/–1.2 γ.

[1] Actually, the data used in preparing figure 4 were obtained by computing the magnetic anomaly as it would appear to a scalar magnetometer transported on a large number of radial approaches toward the ferromagnetic dipole and determining the ranges at which the absolute value of the anomaly equaled 0.03 γ.

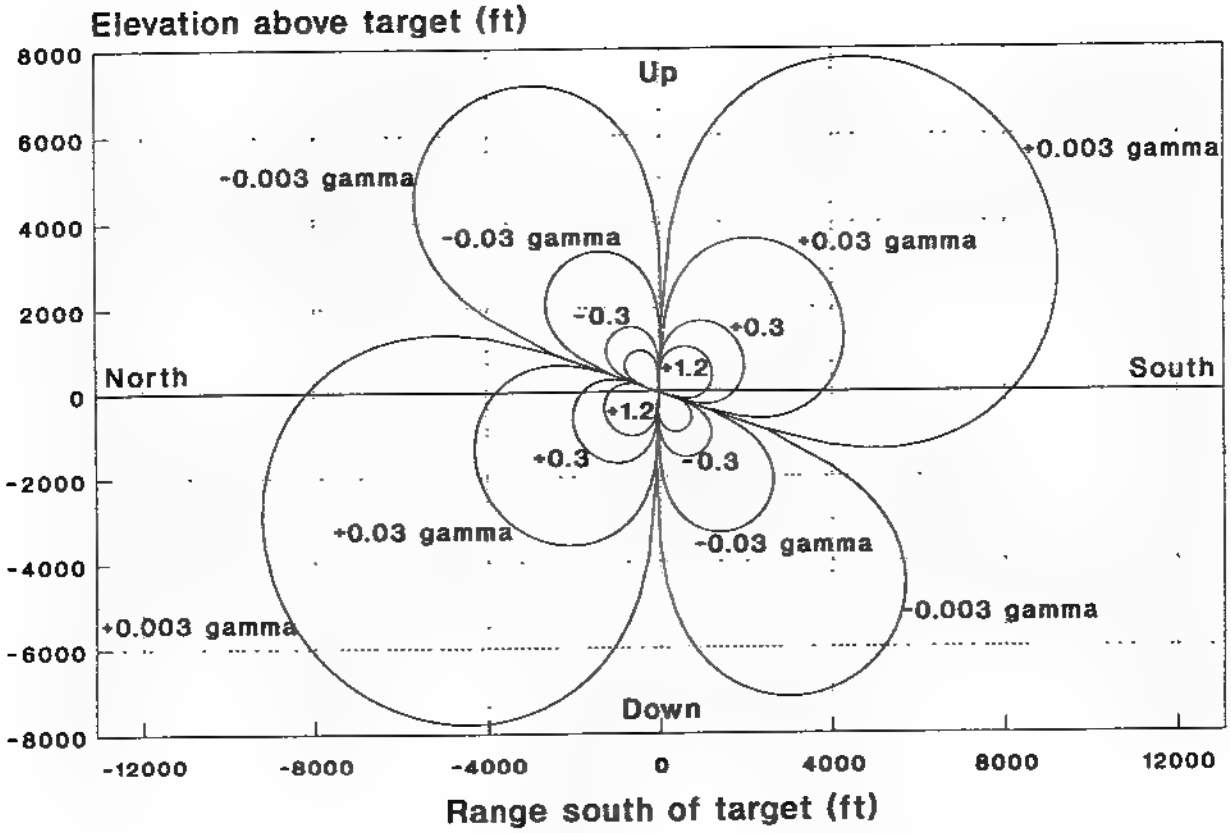

Figure 5. Vertical section of a ferromagnetic anomaly in submarine-fixed coordinates.

Figures 6 and 7 illustrate calculated signatures for a ferromagnetic dipole as they might appear to an airborne magnetometer at 350-ft altitude passing through the anomaly shown in figures 4 and 5. Figure 6 shows signatures from four simulated crossings on easterly courses over the path of the submarine at 150-ft depth on a northerly heading. Curves A and B correspond to passes 3000 ft and 1500 ft north of the submarine whereas curves C and D are the counterpart signatures south of the submarine. The principal feature of curve A is a weak positive value near the point of closest approach to the submarine corresponding to passage near the upper edge of the forward, downward-directed lobe of the anomaly. The path associated with curve B is one that took the simulated sensor first through the negative toroidal portion of the anomaly, then through the positive dumbbell portion, and then out through the eastern portion of the negative toroid. Curves C and D exhibit greater amplitudes than A and B because they correspond to passages near the center of the upward-directed, positive lobe of the dumbbell. Figure 7 shows two signatures; the larger one corresponds to an easterly pass directly over the submarine through the negative toroidal part of the anomaly; the other represents a pass on a northerly course 1000 ft to the west of the submarine. In this latter case, the sensor passes first through the positive, upward-directed lobe of the dumbbell and then through the negative toroid.

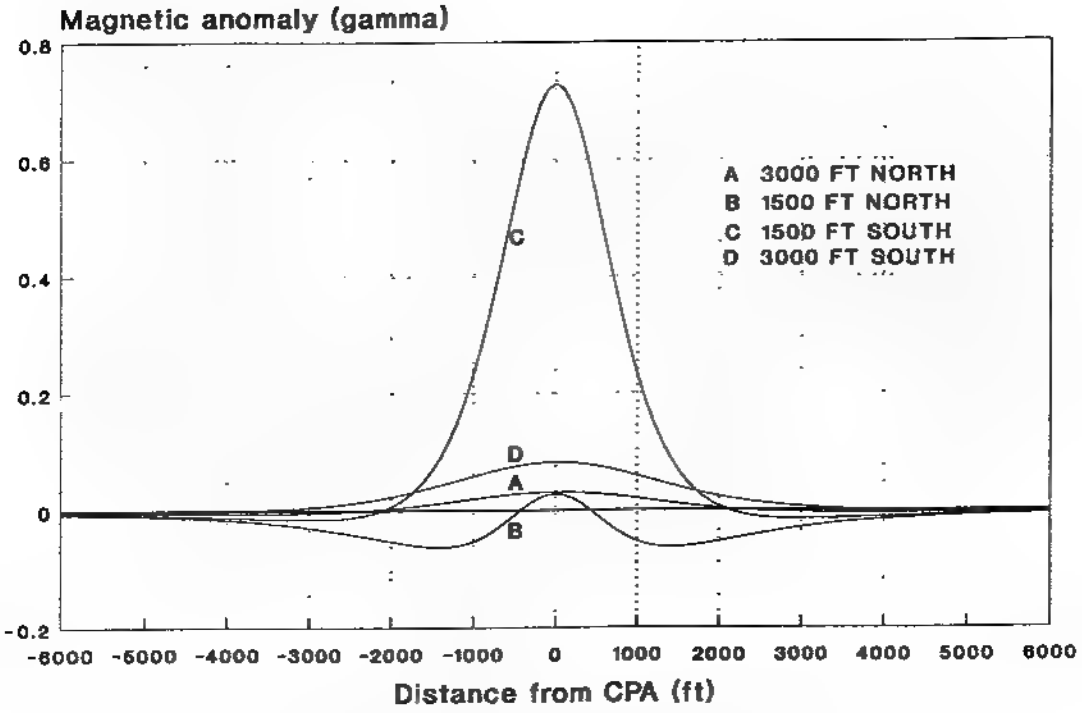

Figure 6. Calculated MAD signatures for sensor aircraft on easterly courses forward and aft of a northbound submarine.

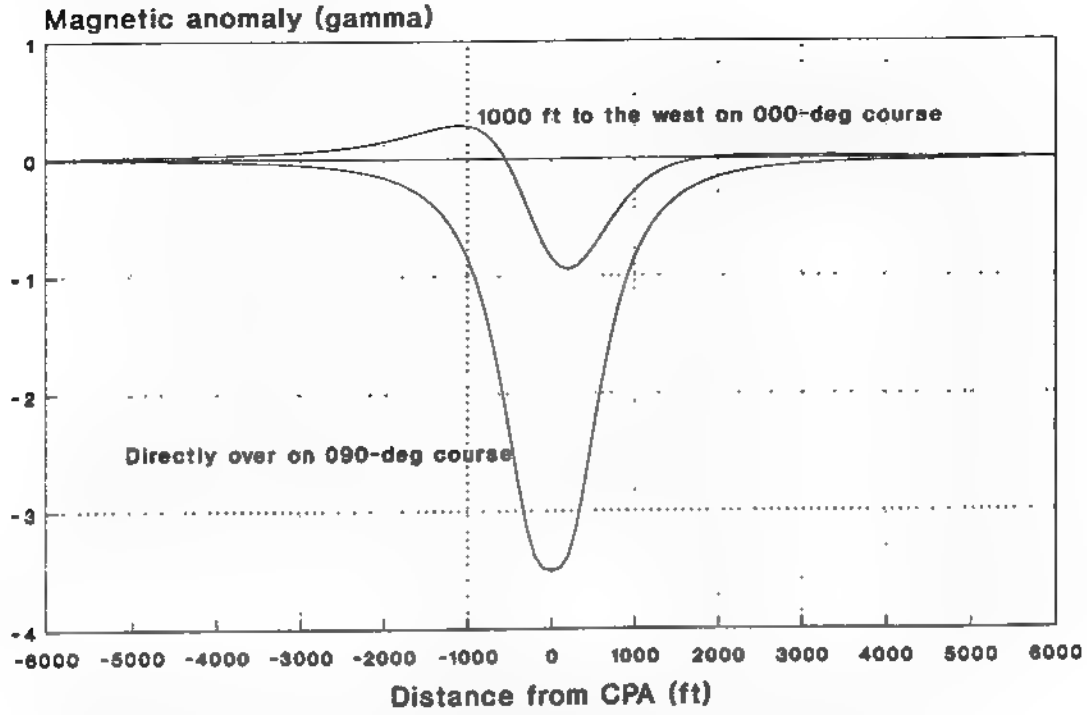

Figure 7. Calculated MAD signatures for sensor aircraft on 090° and 000° passes over/abeam a northbound submarine.

Reference (a) presents more than one hundred plots of calculated submarine anomalies as they would appear to an airborne MAD for various aircraft and submarine headings and encounter geometries.

Figure 8 is a computer-generated, three-dimensional anomaly from a point ferromagnetic anomaly representing the locus of points for which $\Gamma = +/-1\ \gamma$ superimposed to scale on a drawing of a submarine.

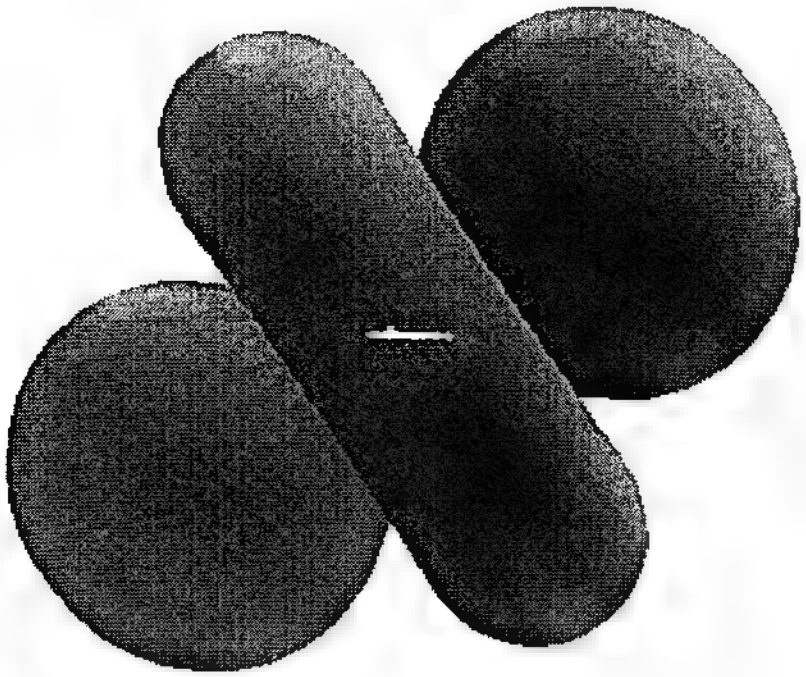

Figure 8. Three-dimensional anomaly surrounding a submarine. The curved surfaces represent the locus of points for which $\Gamma = +/-1\ \gamma$.

Figure 9 provides three views of a computer-generated plot of the ferromagnetic anomaly which would surround a submarine on a north magnetic heading in the Strait of Hormuz where the inclination of the earth's magnetic field is 40.3° (down). The coordinate system is centered at a point ferromagnetic dipole that is assumed to be the magnetic representation of the submarine. The submarine was assumed to possess the following components of magnetic moment:

$$M_{VE} = -7.1 \times 10^8\ \gamma \cdot ft^3 \tag{16}$$

$$M_L = 13.8 \times 10^8\ \gamma \cdot ft^3 \tag{17}$$

$$M_A = 0 \tag{18}$$

$$M = 15.5 \times 10^8\ \gamma \cdot ft^3. \tag{19}$$

The depression angle of the resultant moment vector can be obtained from equations (16) and (17) as $\arctan(M_{VE} / M_L) = 27.2°$. Thus the submarine's moment vector lies at an angle that is between the submarine's longitudinal axis (horizontal) and the direction of the earth's field vector. Figure 9(a) provides a horizontal view looking east; figure 9(b) is a horizontal view viewing north; figure 9(c) is a vertical view from above.

The axis of highest symmetry of the anomaly is oriented at a depression angle of 33.75°, which is mid-way between the magnetic moment vector of the submarine (27.2°) and the earth's field vector (40.3°). A magnetic anomaly detector exhibiting a sensitivity of 0.03 γ would provide a detectable signal anywhere within the closed volume illustrated. Note, in figure 9(a), that a pass of the MAD on an easterly heading directly over the center of the submarine would fail to detect it if the vertical separation exceeds about 2200 ft; however, 2000 ft to the north or the south, detection could be achieved at a vertical separation of 3000 ft. On the other hand, it would be possible to miss a detection 2500 ft north of the submarine at a vertical separation of 1000 ft but to achieve detection by flying 1000 ft higher.

Although equation (7) describes the range R_B at which the magnetic induction from a dipole has the value B_D, without taking into account the earth's field, it still can be used to estimate the radius of the toroidal portion of the anomaly by setting $\theta_R - \theta_M = 90°$ and to estimate the maximum radial extent of the dumbbell portion by setting $\theta_R - \theta_M = 0°$ and solving for R_B. Thus a good approximation of the radius R_{BT} of the toroid is

$$R_{BT} = -(M/B_D)^{1/3} = -(15.5 \times 10^8\ \gamma \cdot ft^3 / 0.03\ \gamma)^{1/3} = -3725\ ft, \qquad (20)$$

and a good approximation of the maximum radial extent R_{BD} of the dumbbell is

$$R_{BD} = (2\ M/B_D)^{1/3} = (2 \times 15.5 \times 10^8\ \gamma \cdot ft^3 / 0.03\ \gamma)^{1/3} = 4693\ ft. \qquad (21)$$

The negative sign in equation (20) may be related to the negative sign of the anomaly within the toroid.

In Appendix B, 36 different horizontal views of the anomaly illustrated in figure 9 are shown as a succession of stereo pair images at 10-degree increments of angle.

In reference (a) it was pointed out that the anomaly from a ferromagnetic dipole as observed with a scalar magnetometer reveals little information about the heading of the target submarine. For example, it was shown that if the submarine has no horizontal permanent component of magnetic moment, the maximum horizontal deviation of its moment from magnetic north would be about 36°. Because the anomaly axis bisects this angle, the maximum deviation of the anomaly would be 18°. If it is assumed that the submarine can possess a horizontal component of permanent magnetic moment that does not exceed about 25% of the maximum induced longitudinal moment, the maximum deviation angle as a function of submarine heading will not exceed 50° and the anomaly will not deviate by more than 25°. Thus, it can be concluded that the anomaly axis of a submarine with no active signature modification equipment will deviate between 18° and 25° from magnetic north as the submarine heading changes over a full 360°. Thus, the ferromagnetic anomaly provides little unambiguous information regarding the heading of the submarine.

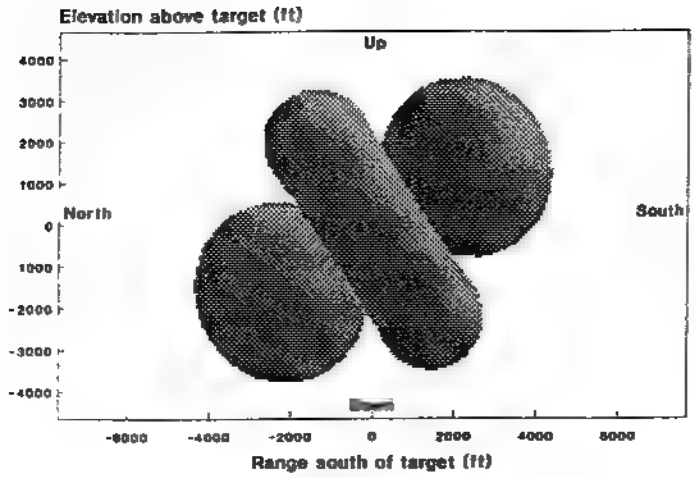

(a)

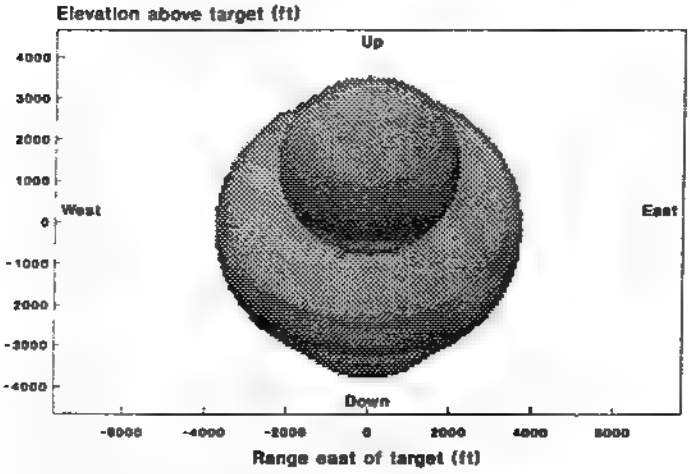

(b)

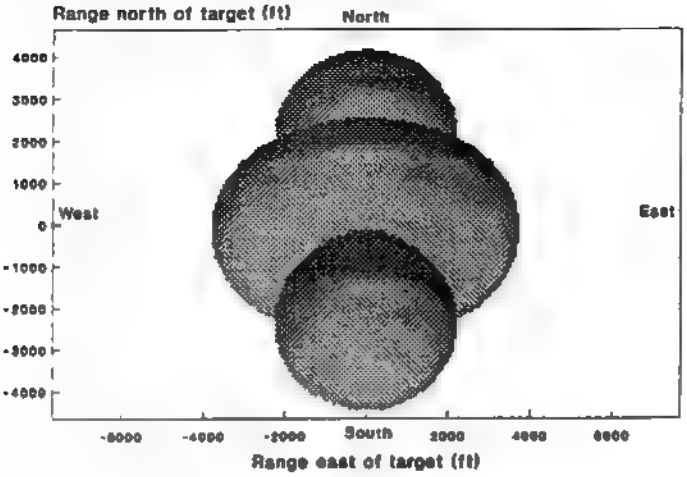

(c)

Figure 9. Computer-generated plots of a ferromagnetic anomaly in submarine-fixed coordinates.

(a) Horizontal view from portside viewing east.
(b) Horizontal view from astern viewing north.
(c) Vertical view from above.

Magnetic Induction and Anomaly from an Extended Ferromagnetic Dipole

For observation distances that are not large in comparison with the length of a submarine, the point dipole assumption breaks down. For handling such cases, it was assumed in reference (a) that a better representation could be obtained by representing the target magnetically as comprising two magnetic poles, an N-pole and an S-pole, separated by a distance equal to about 90% of the length of the submarine. In Appendix D of reference (a), expressions were developed for calculating the magnetic induction from an extended ferromagnetic dipole of arbitrary length, location, and orientation. It was shown that if the distance from the extended dipole to the observation point exceeded several target lengths, the two approaches yielded equivalent results. However, it was also shown that, at short distances, such as those used in making airborne measurements of submarine magnetic moments, considerable error could be introduced by applying the point dipole approximation. For example, in the case of a point dipole, the separation of the extrema of the magnetic anomaly signature is a function of the target-sensor distance at the point of closest approach. (This is consistent with the lobe structure of the anomaly as depicted in figures 3, 4, and 5.) On the other hand, for an extended dipole, the separation of extrema is a function of not only the observation distance, but also the length of the extended dipole. As a consequence, when signatures are analyzed from the point of view of a point dipole, the inferred range to the target and its inferred magnetic moment appear to be greater than they really are.

To compare the anomalies calculated for point and extended ferromagetic dipoles, figures 10 and 11 were plotted of vertical slices of the magnetic anomalies in target coordinates. As before, three-dimensional figures could be generated by rotating these figures about the anomaly axes. Except for scale, figure 10, for a point dipole, is similar to figure 5. Note that for the point dipole, the transitions between the positive lobes and the negative lobes occur along axes that pass through at the dipole itself located at the origin and that the thickness of the toroid is zero at the origin. On the other hand, figure 11 shows the corresponding anomaly for an extended dipole of 215.55-ft length. In this case, the negative "toroid" has a thickness of about 210 ft, or 97% of the dipole length, at the origin.

Figures 12, 13, and 14 show the same data as figures 10 and 11, but plotted in a way that permits easy comparisons between the point and extended dipole anomalies. Note that the distance scales are different in each of these three figures.

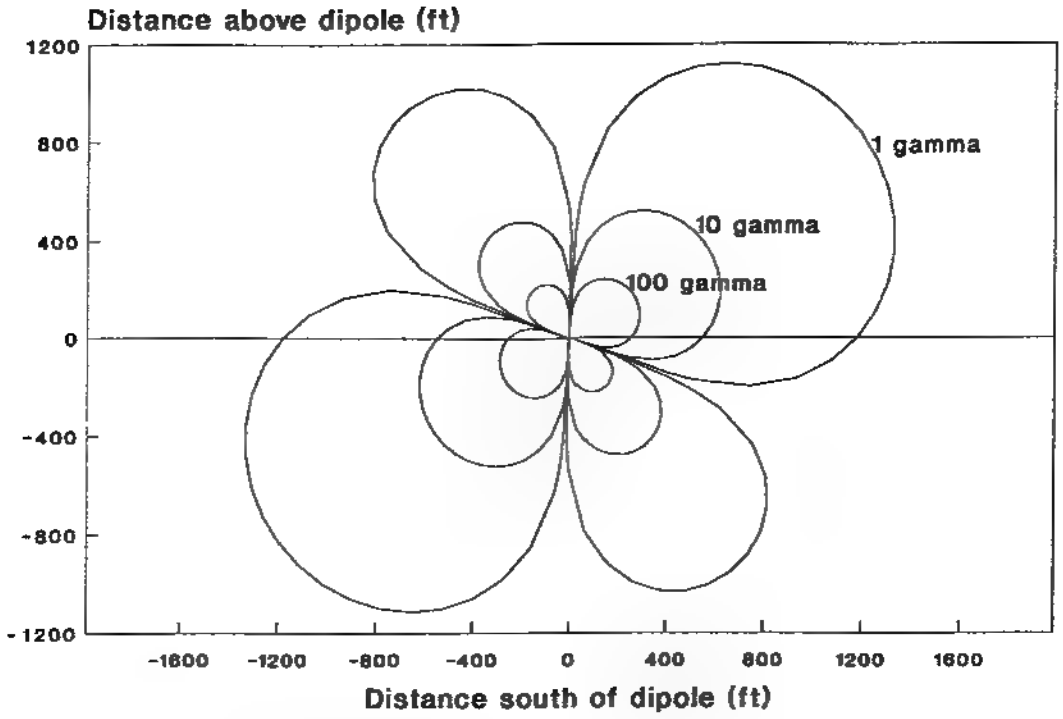

Figure 10. Range at which the anomaly from a point ferromagnetic dipole equals 1, 10, and 100 gamma.

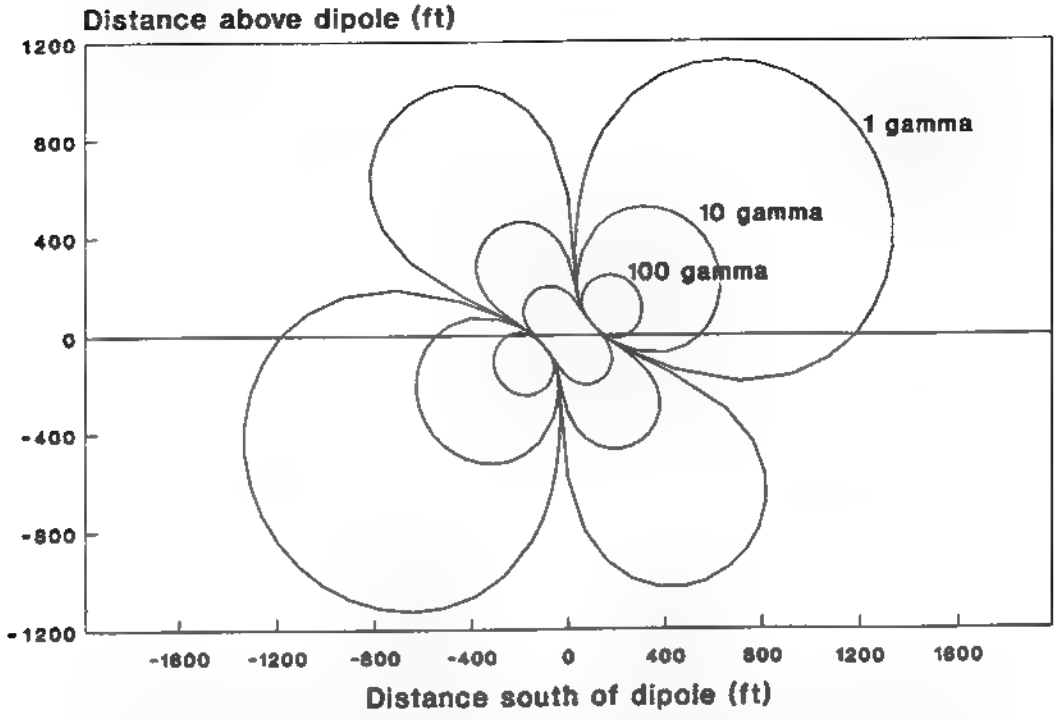

Figure 11. Range at which the anomaly from a 215.55-ft long extended ferromagnetic dipole equals 1, 10, and 100 gamma.

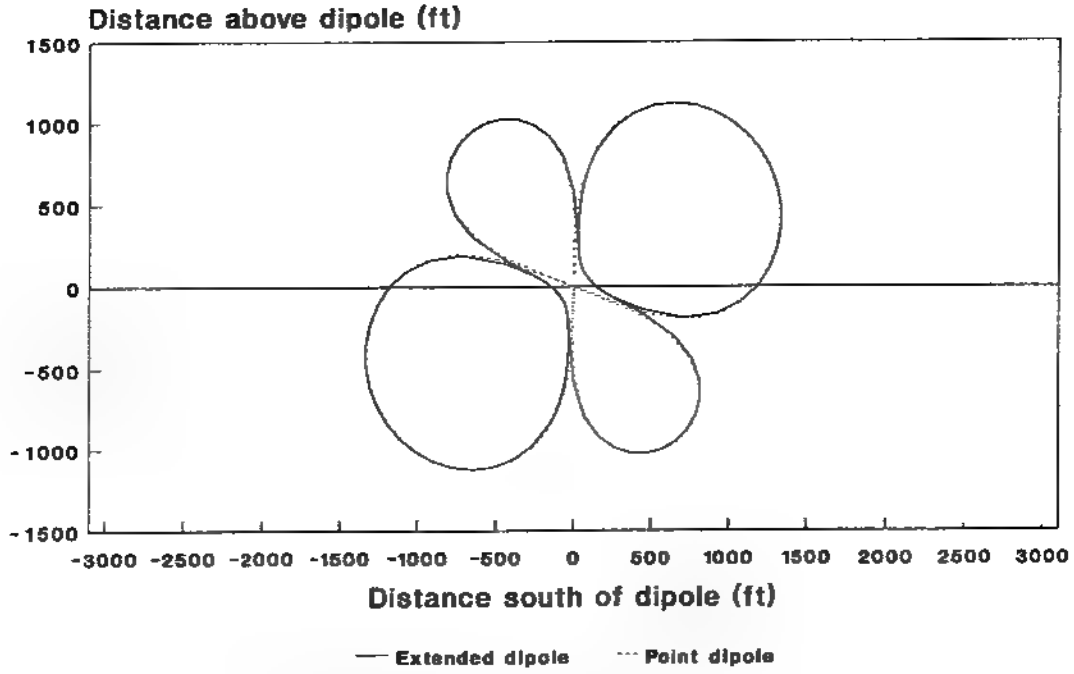

Figure 12. Ranges at which the anomalies from point and extended ferromagnetic dipoles equal 1 gamma.

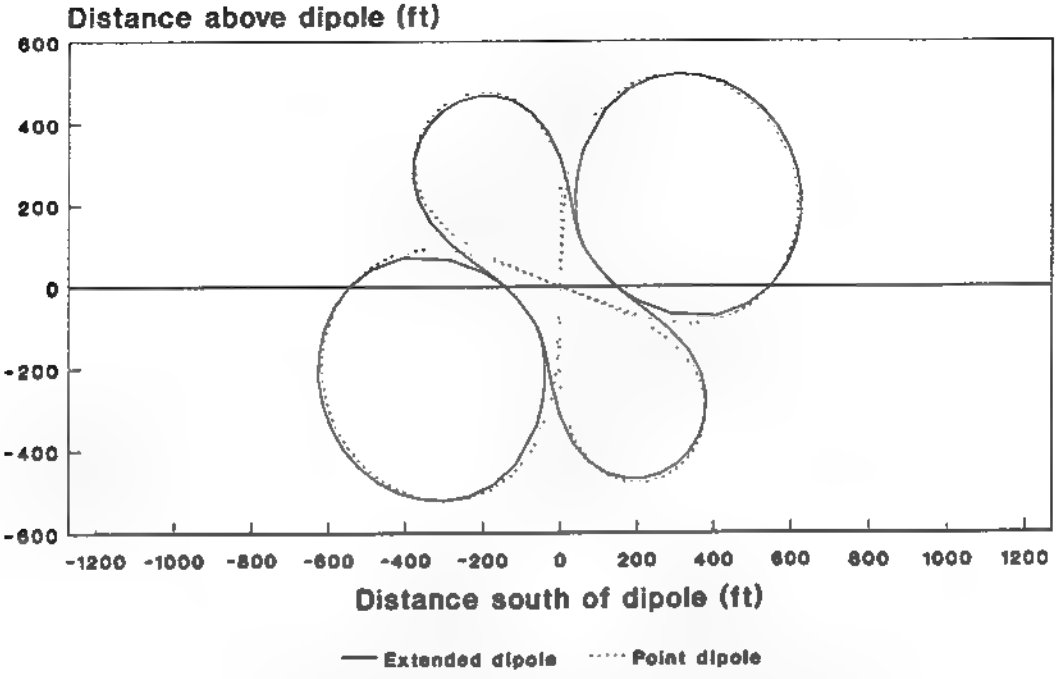

Figure 13. Ranges at which the anomalies from point and extended ferromagnetic dipoles equal 10 gamma.

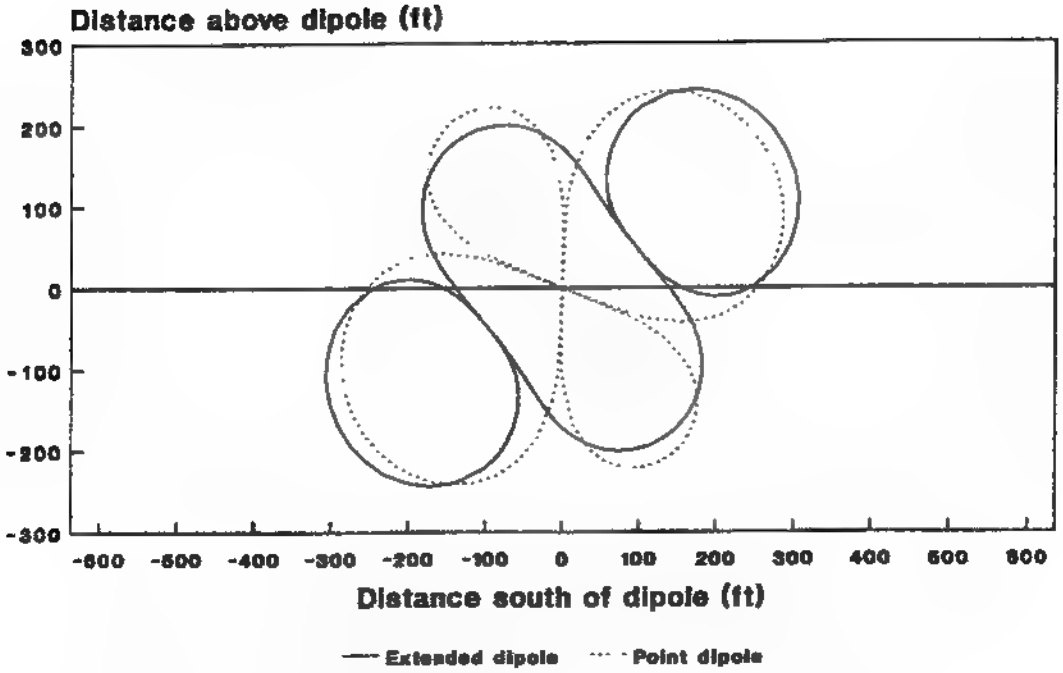

Figure 14. Ranges at which the anomalies from point and extended ferromagnetic dipoles equal 100 gamma.

III. MAGNETIC ANOMALY FROM THE STATIC ELECTRIC CURRENT MOMENT OF A SUBMARINE

As indicated in Section I, a submarine immersed in seawater behaves like a short-circuited galvanic cell. Corrosion currents arise from differences in electric potentials among the interconnected dissimilar metals: copper (in the bronze propeller), iron (in the steel hull) and zinc (in the hull-protecting sacrificial electrodes). The standard electrode potentials of copper, iron and zinc are, respectively, +0.34, –0.44, and –0.76 volt. Thus potential differences of 1.1 V can exist between copper and zinc, 0.78 V between copper and iron, and 0.32 V between iron and zinc. Generally the largest currents flow between the propeller and the nearest zincs, giving rise to a conventional current which flows from the propeller, through the drive shaft, bearings, and hull and then through the water back to the propeller. However, currents may also flow in the opposite direction, particularly in the forward part of the submarine, between the iron in the hull and the zinc blocks. Thus the pattern of electric currents may be very complicated.

In the present analysis it is assumed that the net conventional current in the submarine is forward from the stern toward the bow and the resulting magnetic effects can be described as if they originate from a current source whose dimensions are small compared to the observation distance.

In Appendix C, equations from reference (c) are adapted to the problem of calculating the magnetic anomaly of a submarine arising from galvanic corrosion currents. In reference (a), equations were developed and exercised for calculating the anomaly as it would appear to an airborne scalar magnetometer passing in the vicinity of the submarine. In the present report, the anomaly is presented in submarine-fixed coordinates for both air and seawater surroundings, analogous to the three-dimensional results given in Section II for a ferromagnetic dipole. The anomaly from a ferromagnetic dipole is indifferent to whether the observation is made in air or seawater. This is not the case, however, for the anomaly from a horizontal electric current dipole (HED) assumed to represent the submarine in this context.

Three sets of equations are given in Appendix C, one for the observation point P in air (i.e., altitude $z \geq 0$), another to cover the subsurface situation (i.e., altitude $z \leq 0$), and a third to cover the special simple case of both $z = 0$ and HED depth $-h = 0$. The third set can be obtained from either the first or second set. It will be seen that the HED anomaly is much more complex than that of the ferromagnetic dipole in that there is no axis of rotational symmetry and that the structure is a strong function of the orientation of the HED in the earth's magnetic field.

In figures 15 through 19, the equations of Appendix C (Cases I and II) were used to calculate the locus of points for which the magnetic anomaly Γ from a 100-m deep, static,

1000-A · m HED equals +/–0.01 γ. The assumed location was at 25°N, 58°E in the Gulf of Oman where the components of the earth's magnetic field are

B_{Ey} = 34271 γ (north component)

B_{Ex} = 662 γ (east component)

B_{Ez} = –26582 γ (vertically upward component).

Calculations were performed for two HED headings: 000° magnetic and 090° magnetic. For each HED orientation, +/–0.01-γ contours were plotted: first, a horizontal slice at sea level (z = 0) and then a succession of nine or ten east-west vertical slices at various distances y north and south of the HED.

Figure 15 shows the +/–0.01-γ contours for the 000° magnetic heading of the submarine. Figure 15, a plan view at the sea surface, shows four lobes: positive ones to the southeast and northwest and negative ones to the southwest and northeast. Figures 16(a) through 16(i) show the vertical slices at distances 2600, 2000, 1000, and 0 m south of the HED, and 200, 400, 500, 1000, and 1400 m north of the HED. Roughly equal amounts of the anomaly appear above and below the air-water interface. It is interesting to note that an MAD aircraft flying on a 000° magnetic course directly over the submarine on this 000° magnetic heading would fail to detect its HED anomaly.

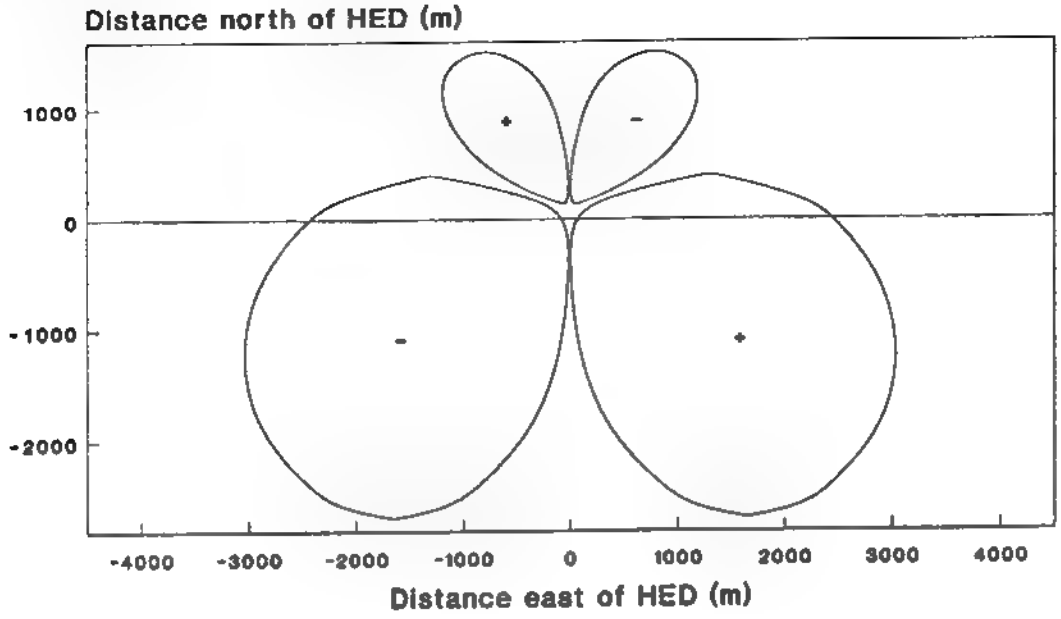

Figure 15. Sea-level horizontal section of magnetic anomaly from a static HED on 000°magnetic heading in submarine-fixed coordinates showing +/–0.01-γ contours.
HED: depth, 100 m; electric current moment, 1000 A · m.
Location: 25°N, 58°E. Earth's magnetic field dip angle: 37.8°.

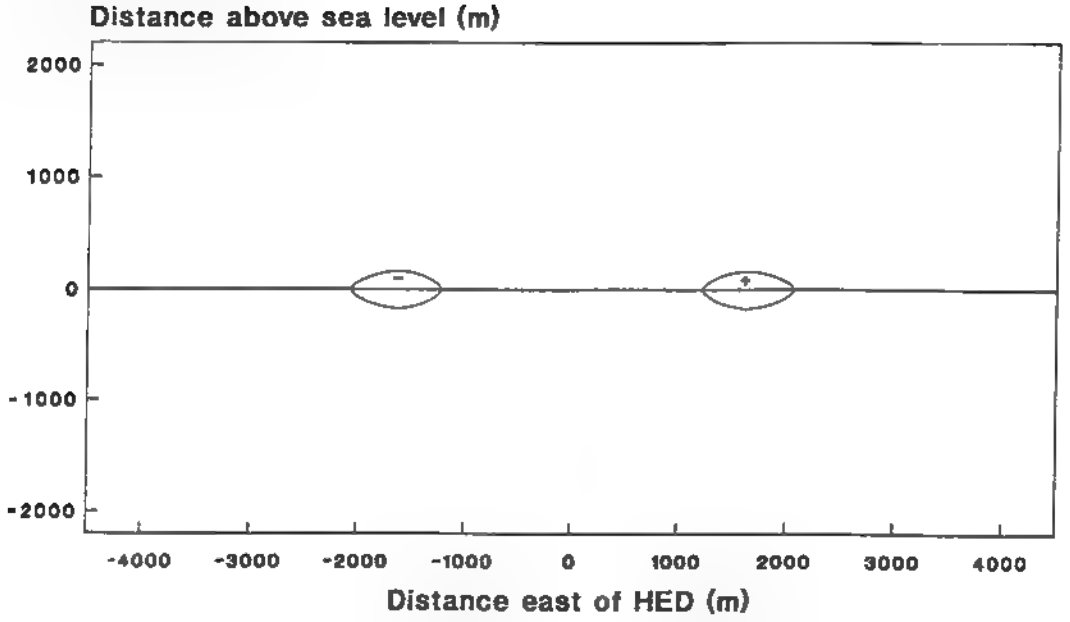

(a)

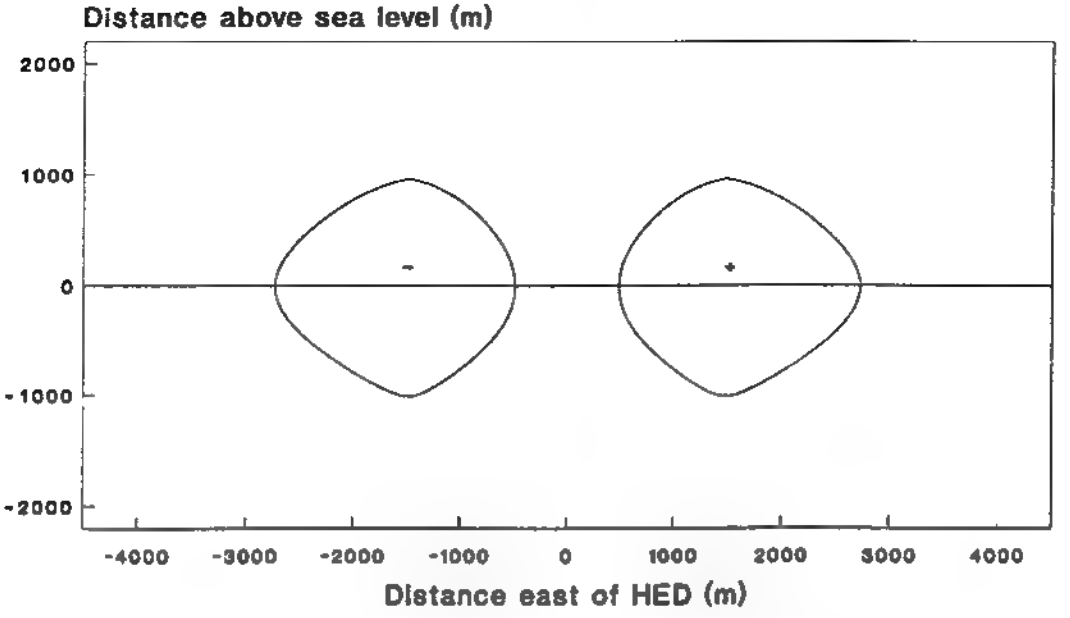

(b)

Figure 16. East-west vertical section of magnetic anomaly from a static HED on 000° magnetic heading in submarine-fixed coordinates showing +/–0.01-γ contours.
(a) 2600 m south of HED (b) 2000 m south of HED
HED: depth, 100 m; electric current moment, 1000 A·m.
Location: 25°N, 58°E. Earth's magnetic field dip angle: 37.8°.

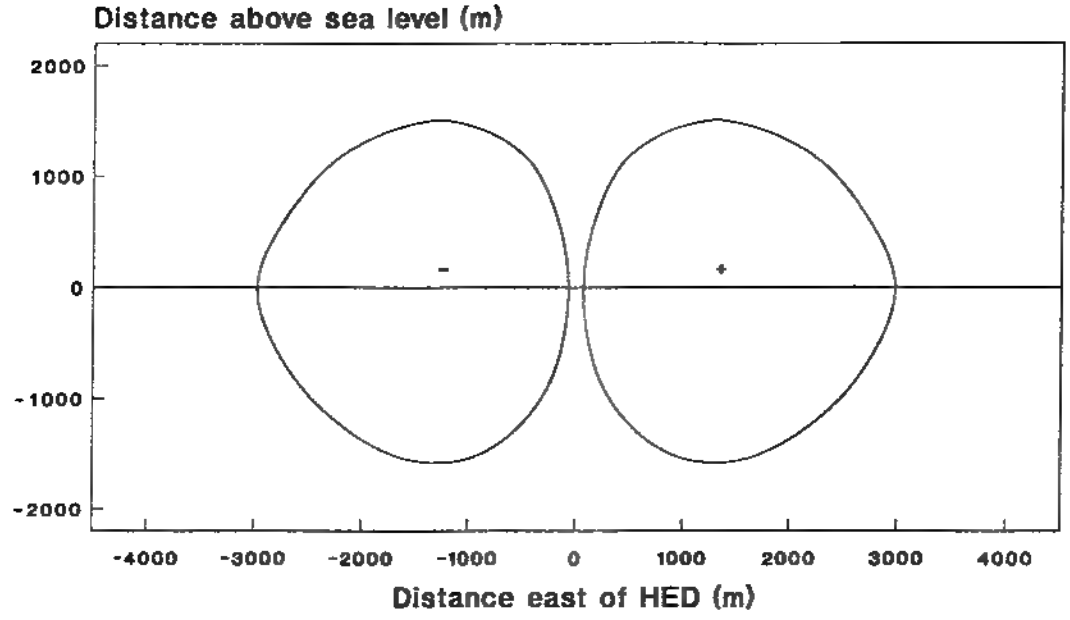

(c)

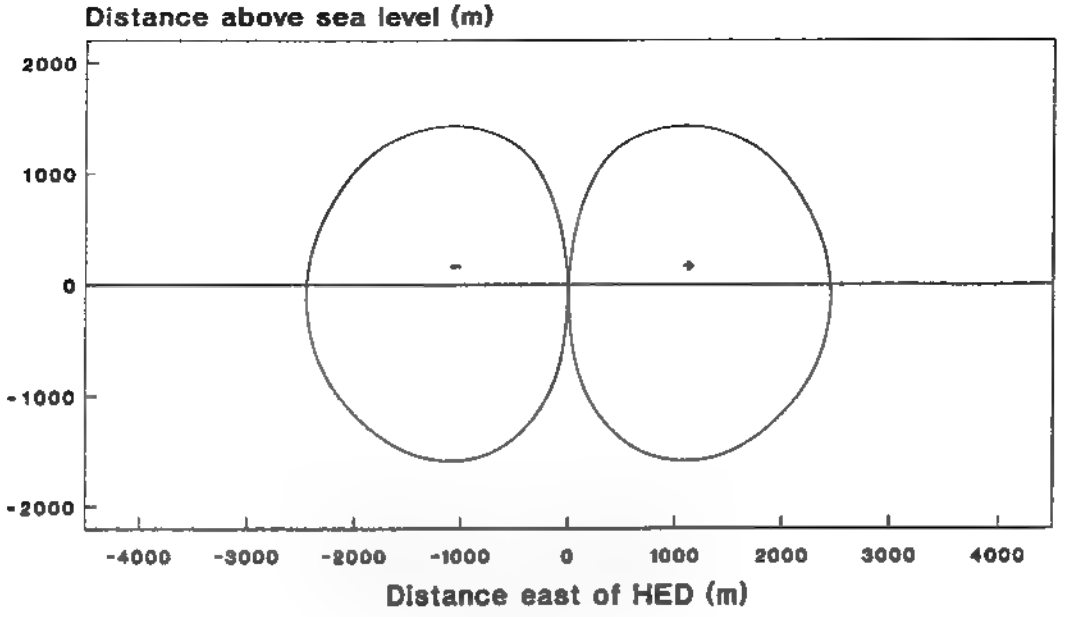

(d)

Figure 16. East-west vertical section of magnetic anomaly from a static HED on 000° magnetic heading in submarine-fixed coordinates showing +/–0.01-γ contours.
(c) 1000 m south of HED (d) 0 m south of HED
HED: depth, 100 m; electric current moment, 1000 A · m.
Location: 25°N, 58°E. Earth's magnetic field dip angle: 37.8°.

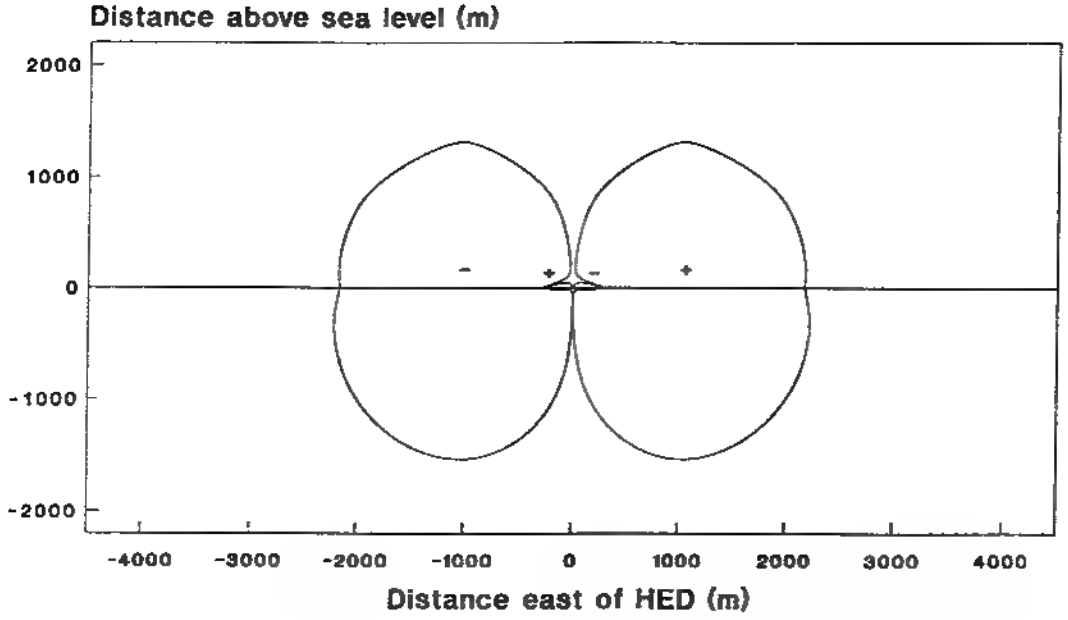

(e)

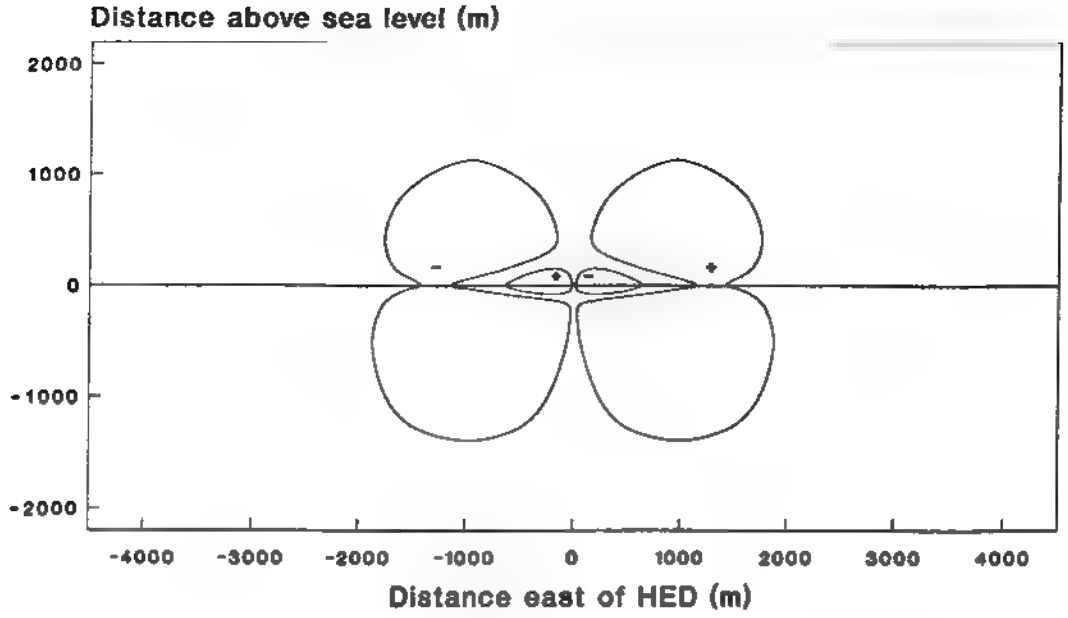

(f)

Figure 16. East-west vertical section of magnetic anomaly from a static HED on 000° magnetic heading in submarine-fixed coordinates showing +/–0.01-γ contours.
(e) 200 m north of HED (f) 400 m north of HED
HED: depth, 100 m; electric current moment, 1000 A·m.
Location: 25°N, 58°E. Earth's magnetic field dip angle: 37.8°.

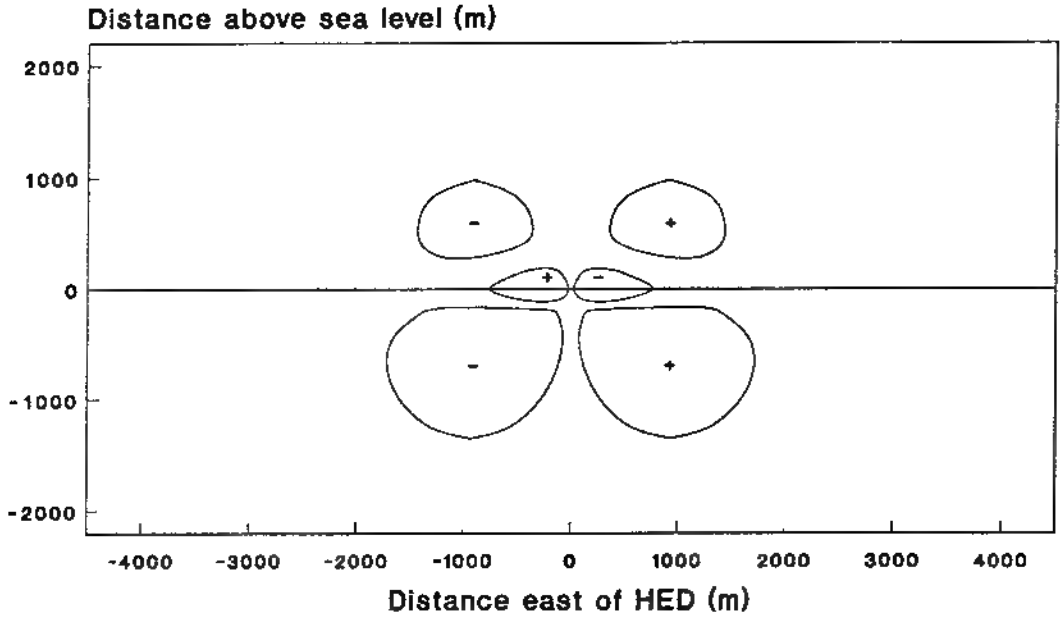

(g)

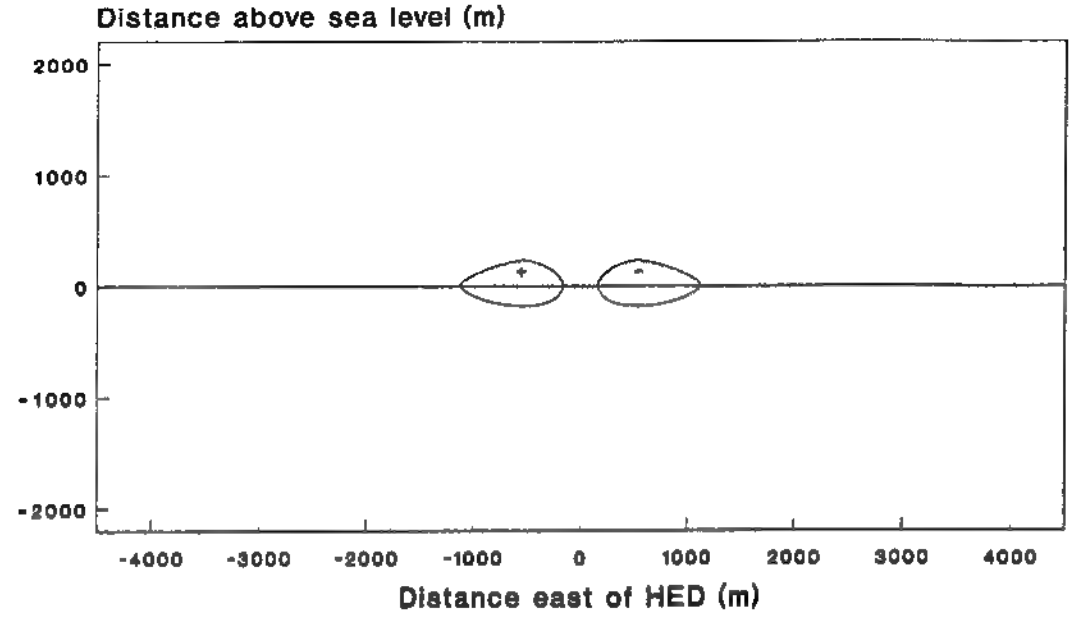

(h)

Figure 16. East-west vertical section of magnetic anomaly from a static HED on 000° magnetic heading in submarine-fixed coordinates showing +/–0.01-γ contours.
(g) 500 m north of HED (h) 1000 m north of HED
HED: depth, 100 m; electric current moment, 1000 A · m.
Location: 25°N, 58°E. Earth's magnetic field dip angle: 37.8°.

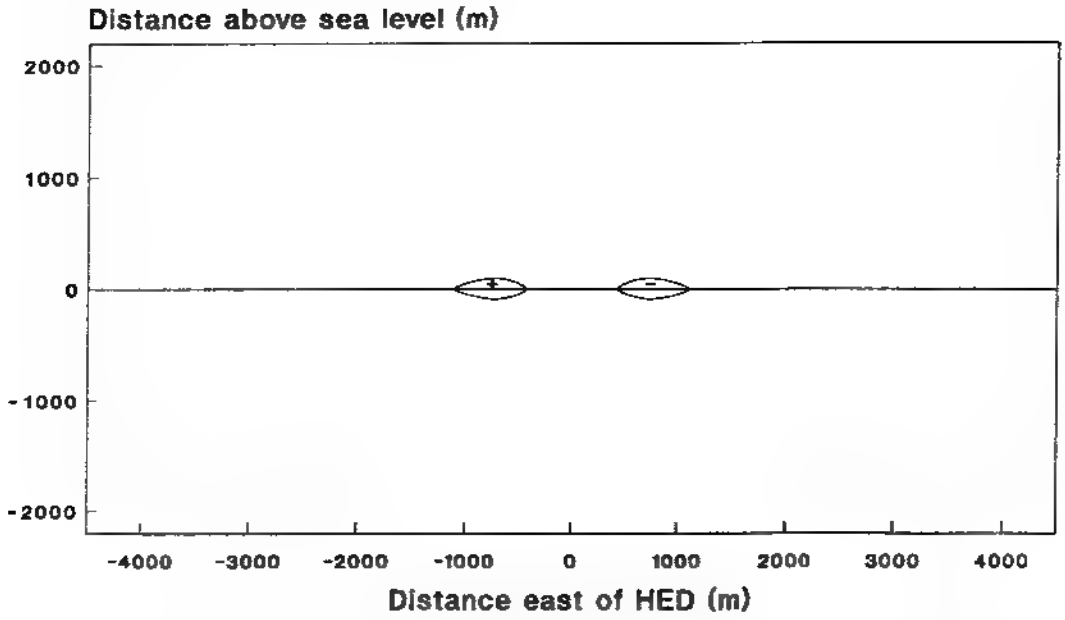

(i)

Figure 16. East-west vertical section of magnetic anomaly from a static HED on 000° magnetic heading in submarine-fixed coordinates showing +/–0.01-γ contours.

(i) 1400 m north of HED

HED: depth, 100 m; orientation, 000° magnetic; electric current moment, 1000 A·m.
Location: 25°N, 58°E. Earth's magnetic field dip angle: 37.8°.

Figure 17 shows the calculated anomaly as it would be observed with an airborne sensor moving from west to east at an altitude of 100 m at a distance of 400 m north of the HED; it should be compared to figure 16(f). Figure 17 may be thought of as one of many traces used to determine the values used in plotting figure 16(f). It shows scale lines indicating the +/–0.01-γ anomaly levels, with markers spaced at distance intervals of 150 m. The anomaly curve crosses the +0.01-γ level at distances –444, –42, +794, and +1630 m east of the HED; similarly, it crosses the –0.01-γ level at distances –1630, –794, +42, and +444 m east of the HED. These same values could, in principle, be read from figure 16(f) by drawing a horizontal line at the 100-m elevation level and noting its eight points of intersection with the curves.

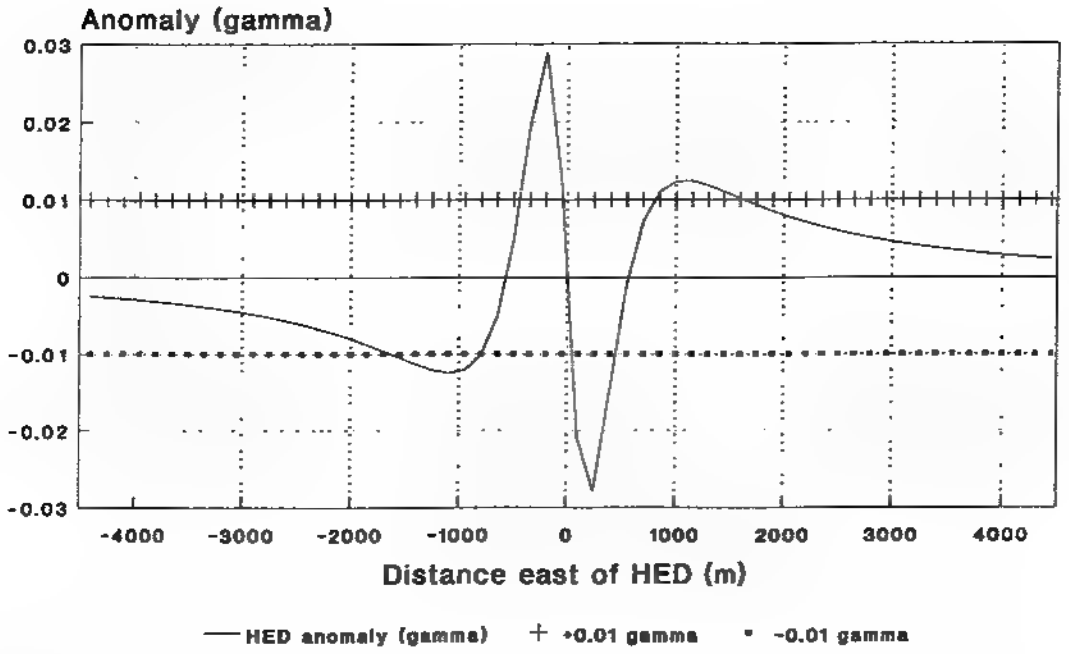

Figure 17. Magnetic anomaly along west-to-east flight path from a static HED in seawater.
Sensor: altitude, 100 m; course, 090° magnetic 400 m north of HED.
HED: depth, 100 m; orientation, 000° magnetic; electric current moment, 1000 A · m.
Location: 25°N, 58°E. Earth's magnetic field dip angle: 37.8°.

Figure 18 shows the +/–0.01-γ contours for the 090° magnetic heading of the submarine. Figure 18, a plan view at the sea surface, shows three lobes: a positive one to the south and negative ones to the northwest and northeast. Figures 19(a) through 19(j) show the vertical slices at distances 3500, 3000, 2000, 1000, 500, 250, and 0 m south of the HED, and 1000, 1400, and 1600 m north of the HED. For this geometry, the positive lobe of the anomaly appears mostly below sea level and the negative portion above sea level.

The parameter values chosen for exercising this model (i.e., p = 1000 A · m and Γ = +/–0.01 γ) are rather optimistic from the detection point of view. Because the static HED anomaly exhibits a generally inverse square law dependence on range, reducing the ratio p/Γ by a factor of 100 (e.g., to more realistic values of p = 100 A · m and Γ = +/–0.1 γ) would reduce detection ranges to about 10% of those implied in figures 15 and 18.

The static HED anomaly offers two significant advantages provided the sensitivity of airborne magnetometers can be improved to exploit it: (1) Because of the inverse square law fall-off with range (as opposed to the inverse cube law fall-offs for the ferromagnetic dipole anomaly and for the alternating HED anomaly), greater detection ranges are potentially available. (2) Because the static HED anomaly is much more strongly dependent upon the heading of the submarine than is the ferromagnetic dipole anomaly, the former provides a much greater opportunity for obtaining tactical information than the latter.

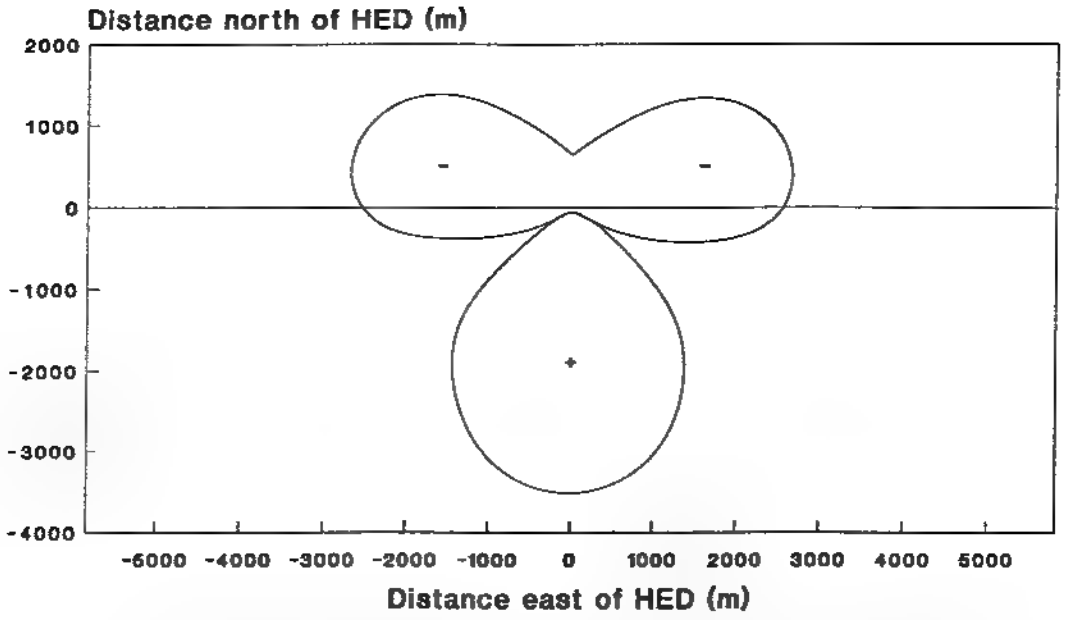

Figure 18. Sea-level horizontal section of magnetic anomaly from a static HED on 090° magnetic heading in submarine-fixed coordinates showing +/–0.01-γ contours.
HED: depth, 100 m; electric current moment, 1000 A·m.
Location: 25°N, 58°E. Earth's magnetic field dip angle: 37.8°.

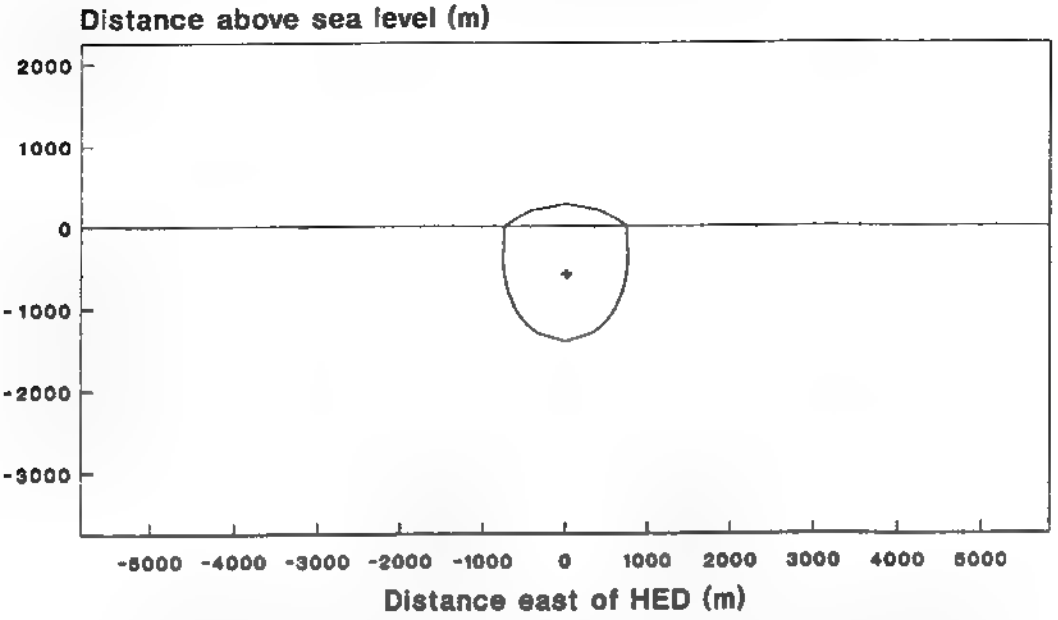

(a)

Figure 19. East-west vertical section of magnetic anomaly from a static HED on 090° magnetic heading in submarine-fixed coordinates showing +/–0.01-γ contours.
(a) 3500 m south of HED
HED: depth, 100 m; electric current moment, 1000 A·m.
Location: 25°N, 58°E. Earth's magnetic field dip angle: 37.8°.

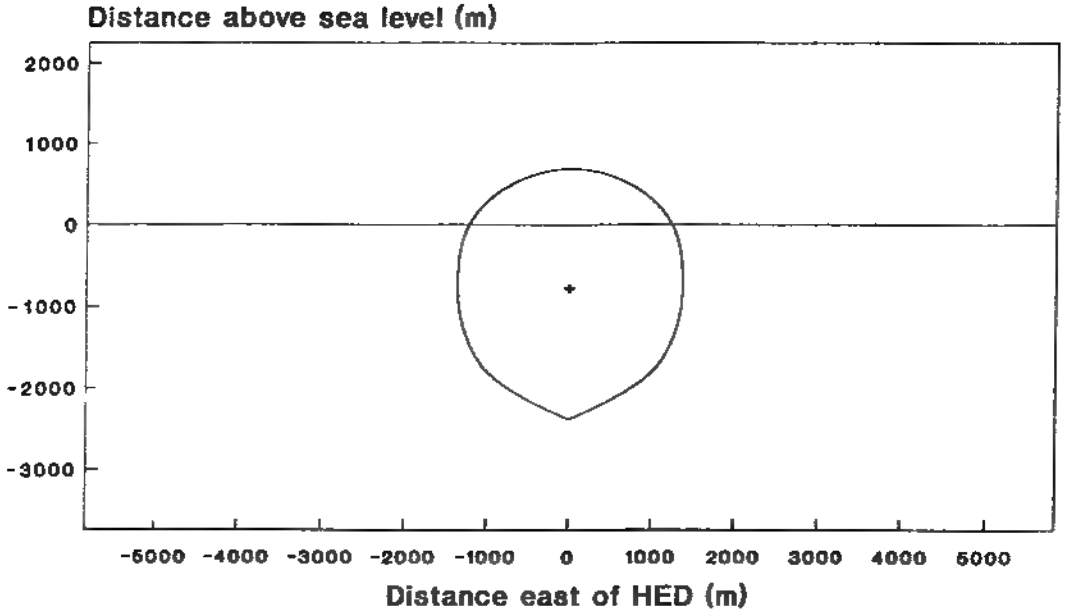

(b)

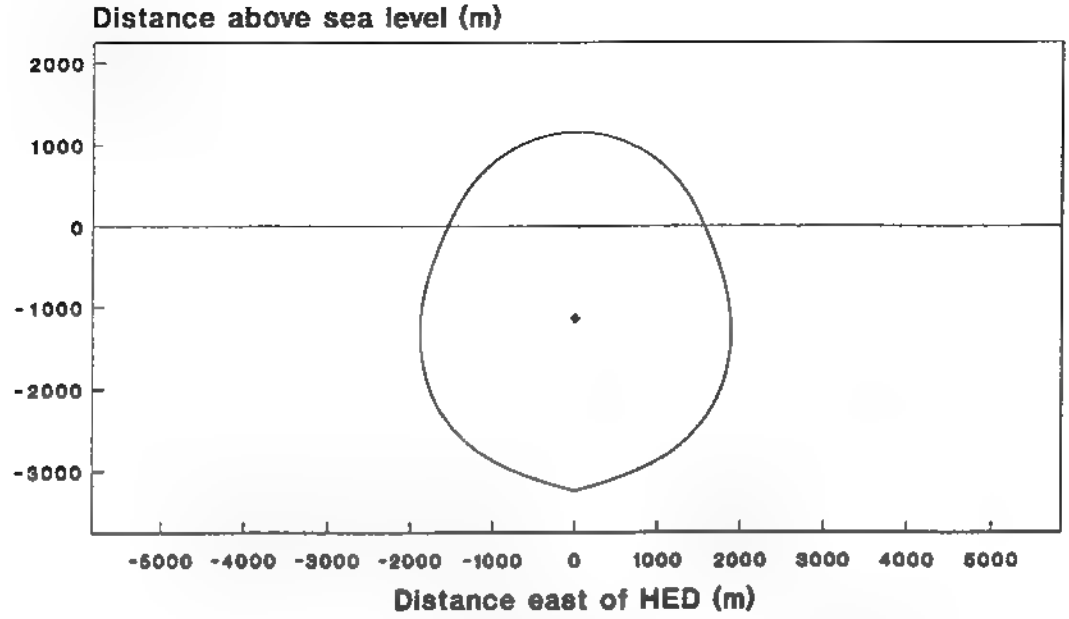

(c)

Figure 19. East-west vertical section of magnetic anomaly from a static HED on 090° magnetic heading in submarine-fixed coordinates showing +/–0.01-γ contours.
(b) 3000 m south of HED (c) 2000 m south of HED
HED: depth, 100 m; electric current moment, 1000 A·m.
Location: 25°N, 58°E. Earth's magnetic field dip angle: 37.8°.

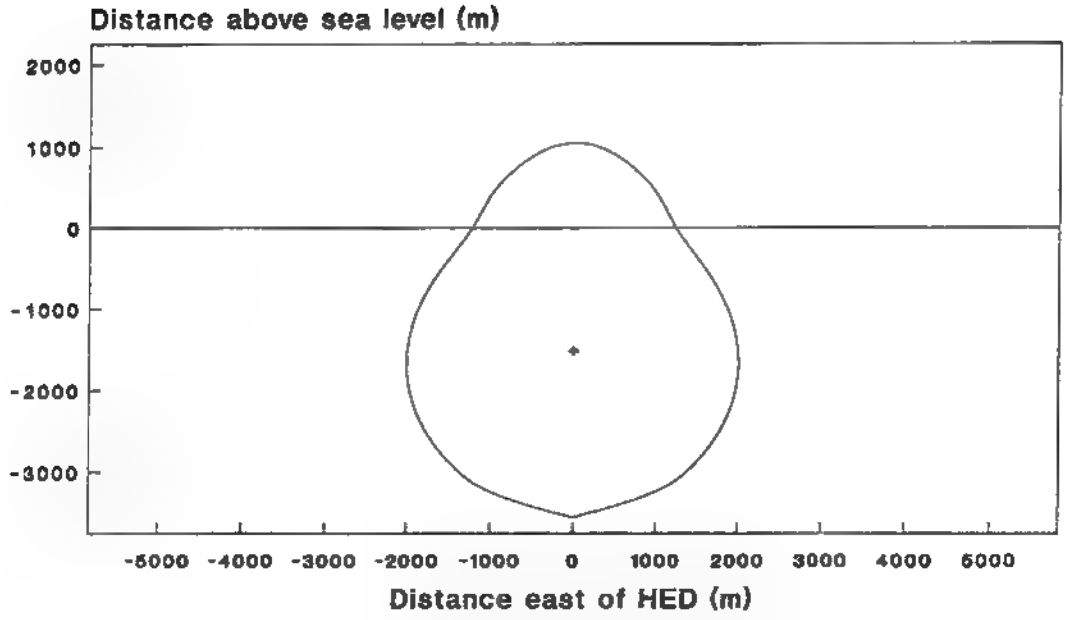

(d)

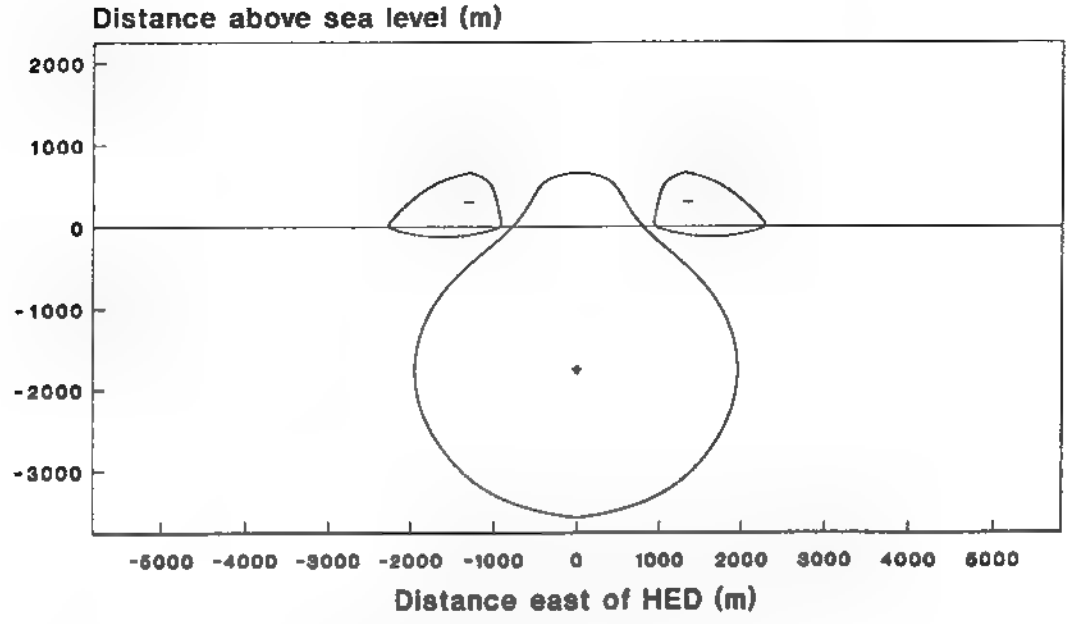

(e)

Figure 19. East-west vertical section of magnetic anomaly from a static HED on 090° magnetic heading in submarine-fixed coordinates showing +/–0.01-γ contours.
(d) 1000 m south of HED (e) 500 m south of HED
HED: depth, 100 m; electric current moment, 1000 A·m.
Location: 25°N, 58°E. Earth's magnetic field dip angle: 37.8°.

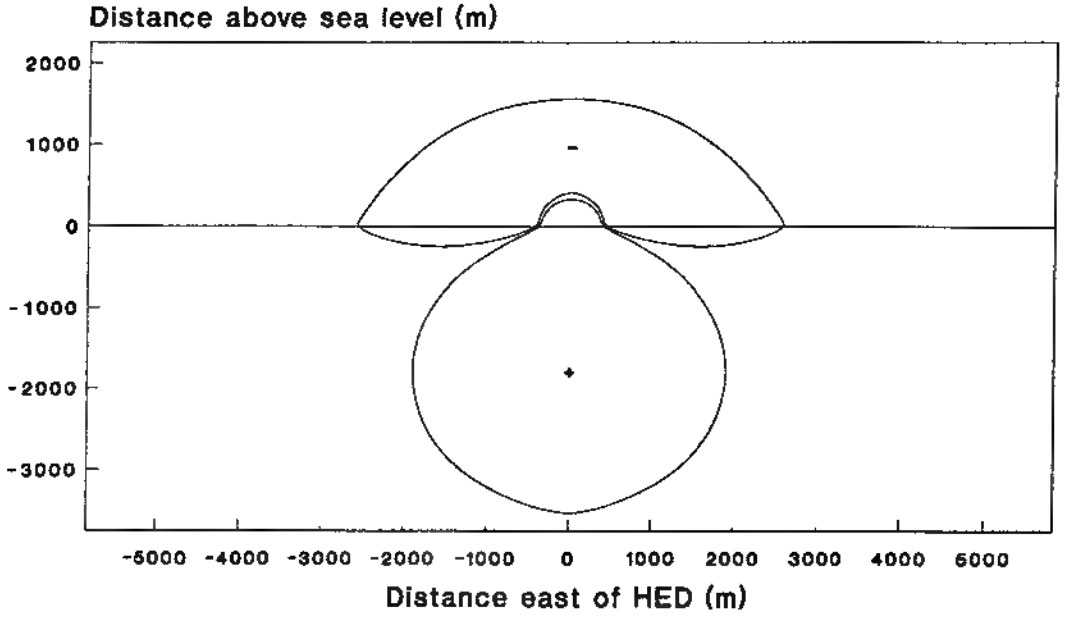

(f)

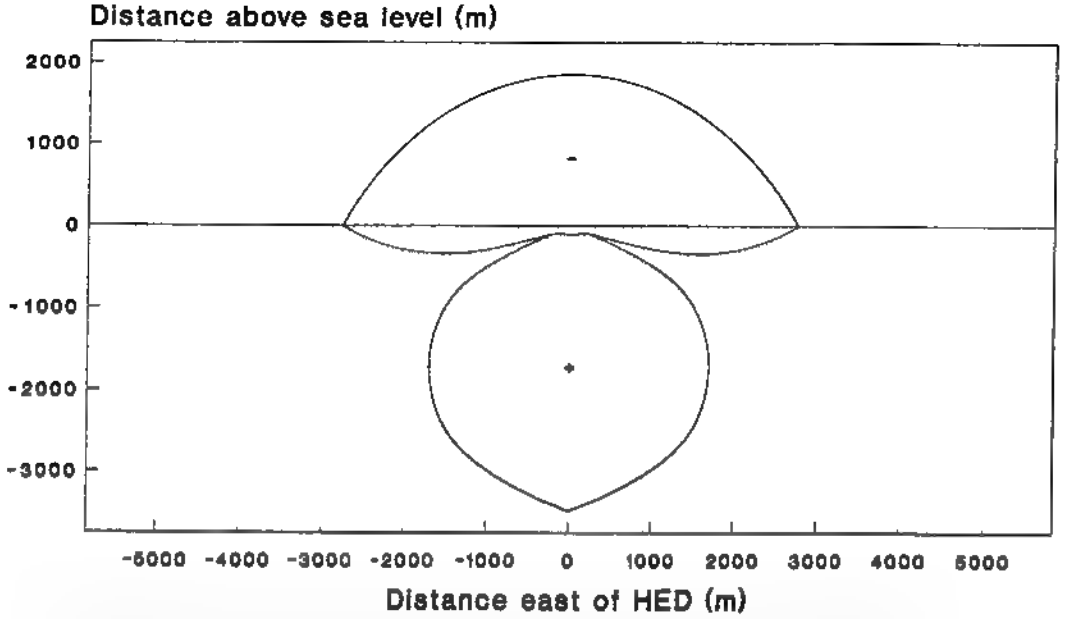

(g)

Figure 19. East-west vertical section of magnetic anomaly from a static HED on 090° magnetic heading in submarine-fixed coordinates showing +/−0.01-γ contours.
(f) 250 m south of HED (g) 0 m south of HED
HED: depth, 100 m; electric current moment, 1000 A·m.
Location: 25°N, 58°E. Earth's magnetic field dip angle: 37.8°.

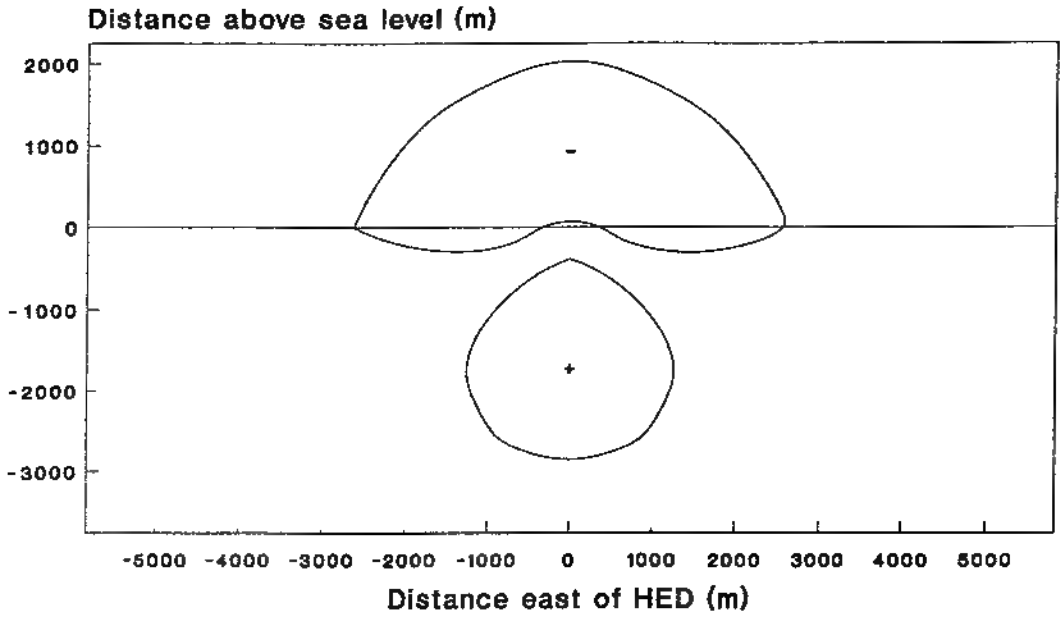

(h)

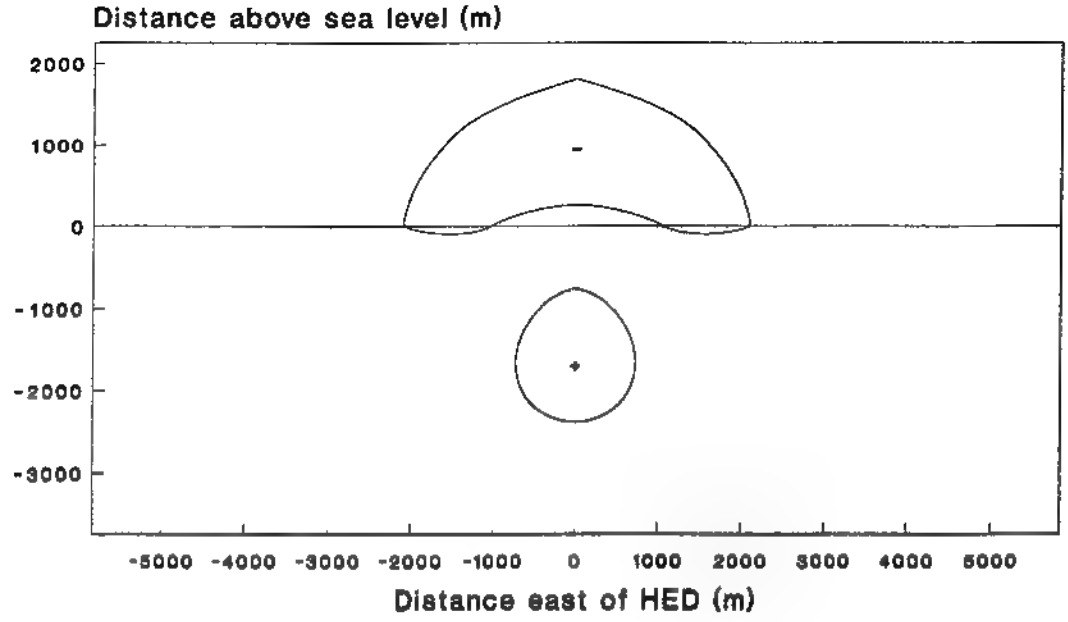

(i)

Figure 19. East-west vertical section of magnetic anomaly from a static HED on 090° magnetic heading in submarine-fixed coordinates showing +/–0.01-γ contours.
(h) 1000 m north of HED (i) 1400 m north of HED
HED: depth, 100 m; electric current moment, 1000 A·m.
Location: 25°N, 58°E. Earth's magnetic field dip angle: 37.8°.

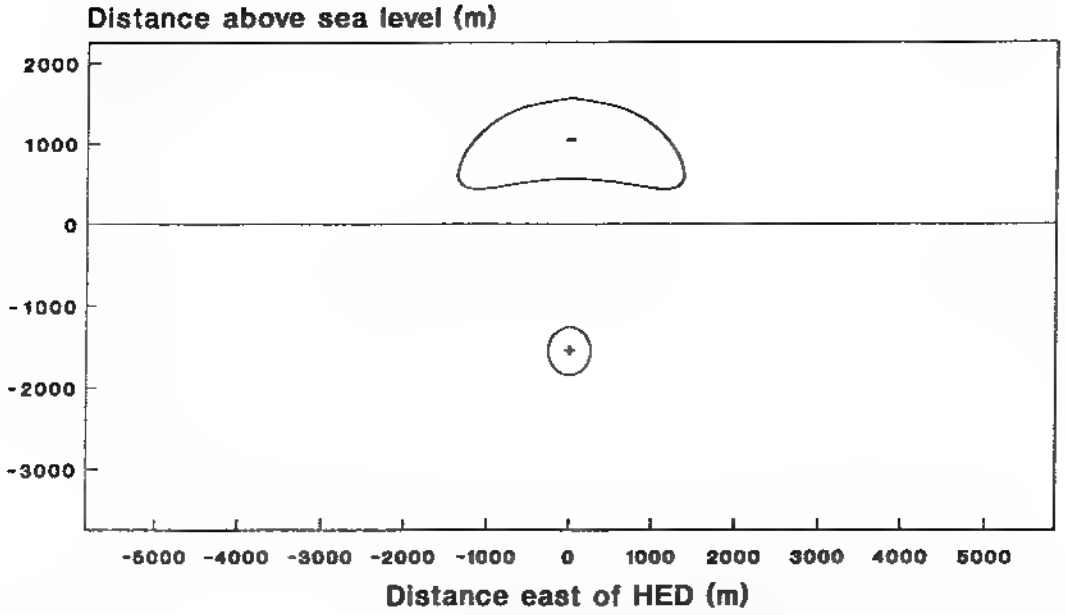

(j)

Figure 19. East-west vertical section of magnetic anomaly from a static HED on 090° magnetic heading in submarine-fixed coordinates showing +/–0.01-γ contours.
(j) 1600 m north of HED
HED: depth, 100 m; electric current moment, 1000 A · m.
Location: 25°N, 58°E. Earth's magnetic field dip angle: 37.8°.

Equations (C-8) through (C-13) can be combined to yield an equation for calculating the magnetic anomaly Γ in a horizontal, sea-level plane from a static HED also at sea level:

$$\Gamma = [100\ p_s /(\rho^2\ B_E)]\ [B_{Ex} \sin(\phi - \theta) - B_{Ey} \cos(\phi + \theta) + B_{Ez} \sin \phi]. \qquad (22)$$

Note that, for this special case, at any given angle, Γ varies as $1/\rho^2$.

Equation (22) can be solved easily for ρ and plotted as a function of compass bearing to field point P for any given value of Γ. Figure 20 is the locus of points for which the magnetic anomaly from a 1000 A · m-HED equals +/–0.01 gamma for a variety of HED headings. The first panel in figure 20A, for which the HED heading is 000° magnetic, is the counterpart of figure 15. Note that figure 15 consists of four distinct closed curves which are not conjoined whereas figure 20A consists of similar closed curves which are conjoined at the origin. The reason for this difference is that the HED was at a depth of 100 meters for the former but at the air-sea interface for the latter. There is a similar relation between the fourth panel of figure 20A and figure 18 for a heading of 090° magnetic. Note that a small positive lobe appears at the surface when the HED depth is zero but not when it is 100 m. (This lobe disappears at an HED depth of 61 m.) Note also in figure 20 that the HED anomaly rotates 180° for 360° of change in submarine heading and that the relative sizes of the lobes vary with rotation, with the southernmost lobe being the largest.

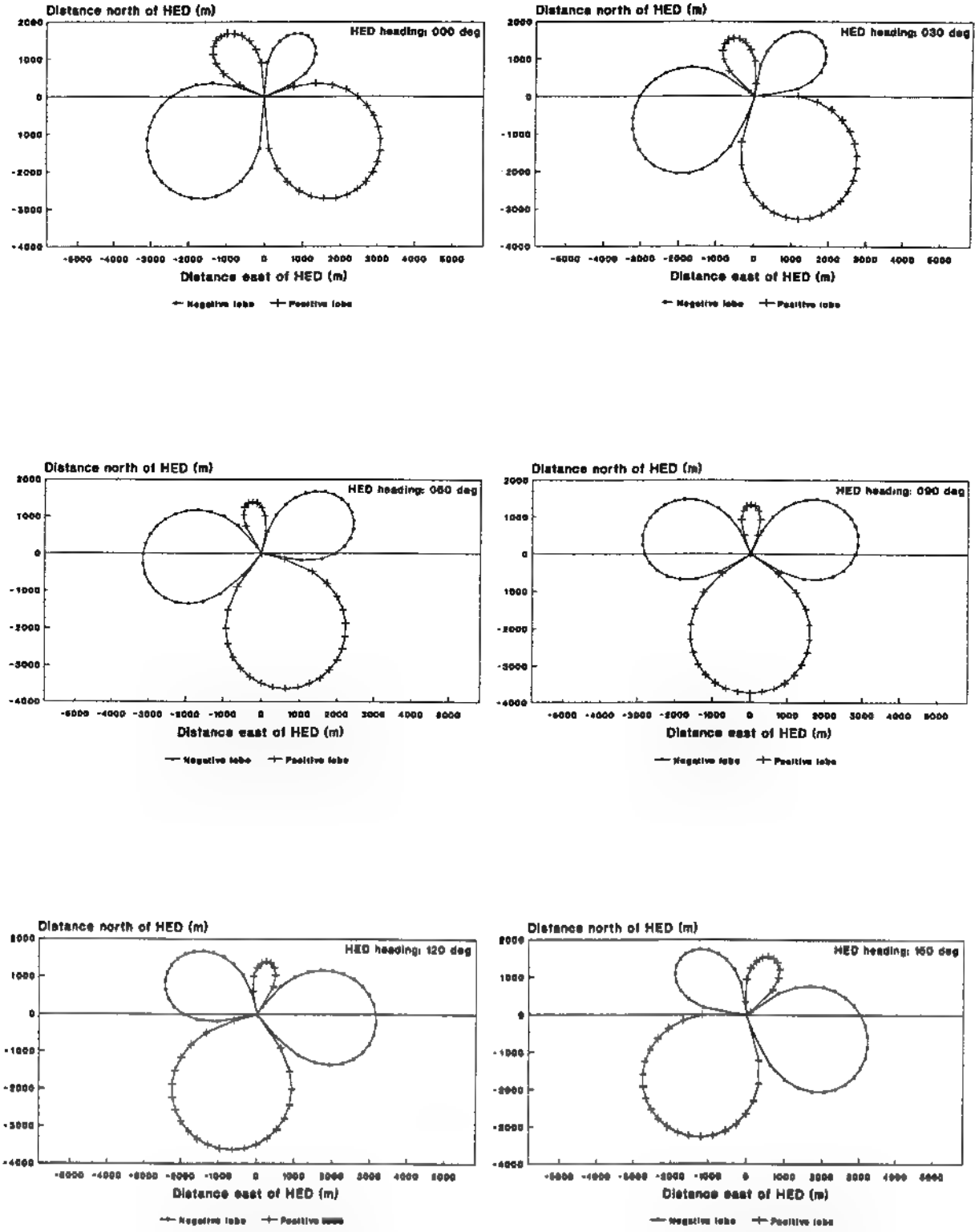

Figure 20A. Magnetic anomaly at the sea surface, represented as +/–0.01-γ contours in submarine-fixed coordinates, from a 1000-A · m static HED at the sea surface for six headings of the submarine.

Submarine headings: 000, 030, 060, 090, 120, and 150 degrees magnetic.

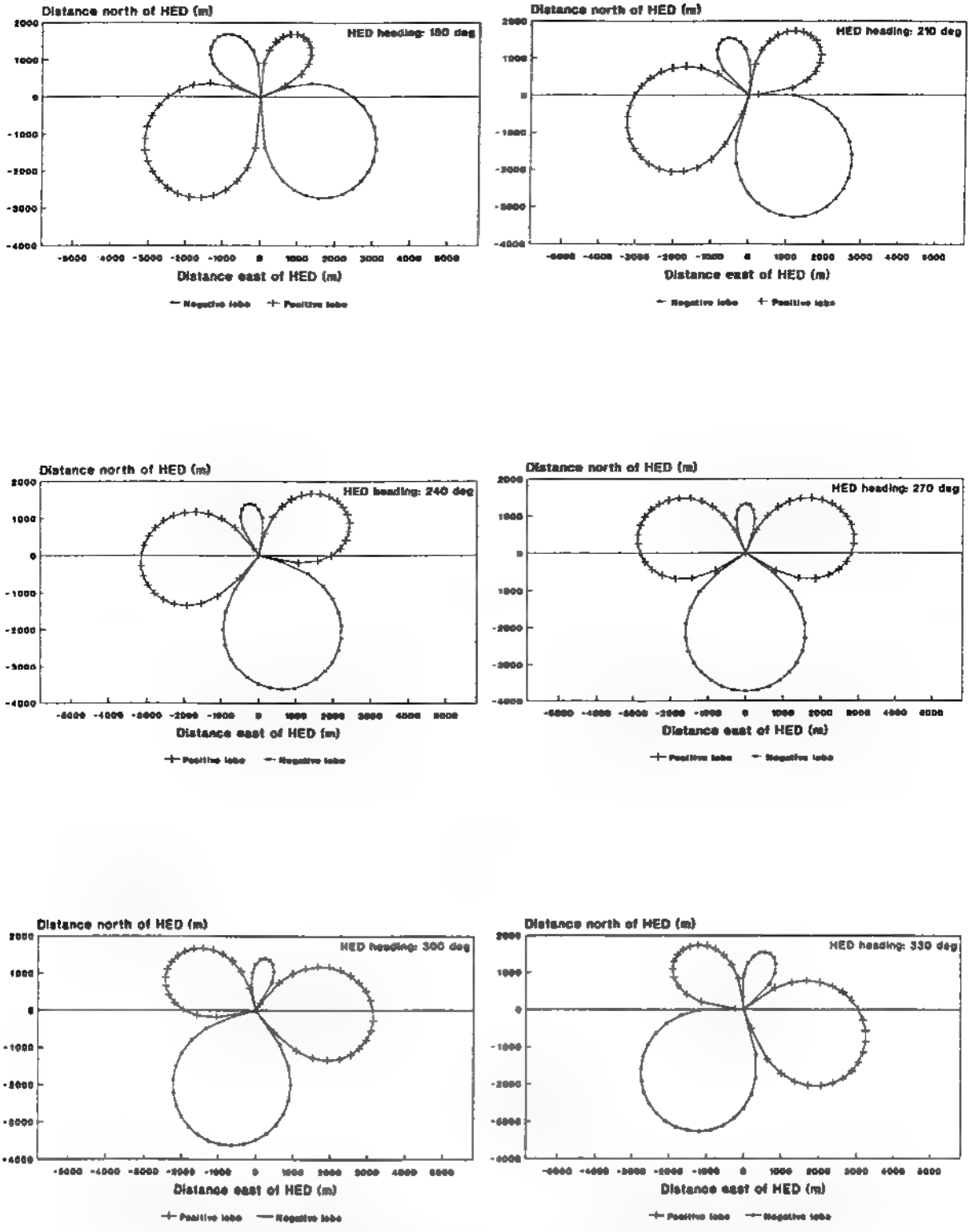

Figure 20B. Magnetic anomaly at the sea surface, represented as +/−0.01-γ contours in submarine-fixed coordinates, from a 1000-A · m static HED at the sea surface for six headings of the submarine.

Submarine headings: 180, 210, 240, 270, 300, and 330 degrees magnetic.

The inverse square law range dependence of the anomaly from a sea-level, static-HED anomaly observed at sea level is illustrated in figure 21. For this set of curves, three ratios of electric current moment and magnetometer sensitivity were assumed: 10^5, 10^4, and 10^3 A · m/γ, corresponding to combinations of source-strength/sensitivity ratios as great as 1000 A · m / 0.01 γ to as small as 100 A · m / 0.1 γ. The linear dimensions of successive lobes are larger by a factor of $10^{1/2}$ (3.16). In a realistic situation, the smaller lobes would probably be swamped by the ferromagnetic anomaly, which follows an inverse cube law dependence; however, at the longer ranges consistent with larger HED moments and greater equipment sensitivities, the HED anomaly would dominate.

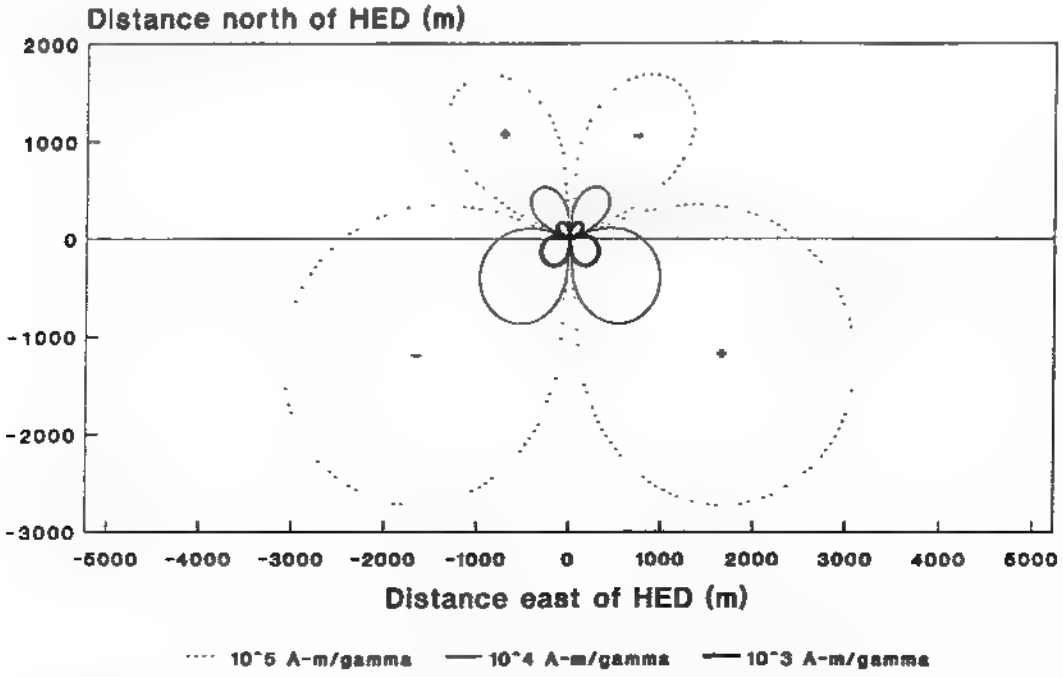

Figure 21. Magnetic anomaly in submarine-fixed coordinates for three ratios of static HED electric current moment and magnetometer sensitivity: 10^5, 10^4, and 10^3 A · m/γ.

The dependence of the appearance of the static HED anomaly upon geographical location is illustrated in figures 22, 23, and 24, which correspond, respectively, to magnetic latitudes of 000° (magnetic equator), 045° (mid-latitude), and 090° (near the north magnetic pole). In each case, the heading of the HED is 000° magnetic and it is positioned at the sea surface; the anomaly is that observed at sea level. The anomaly may be visualized as the surface expression of a tilting three-dimensional figure whose southern portion emerges from the sea with increasing latitude while the northern portion submerges. Near the north magnetic pole, only the previously southernmost lobes appear at the surface. Near the magnetic pole, the anomaly rotates about its vertical axis at the same rate as the HED heading changes whereas near the magnetic equator, it rotates at half that rate.

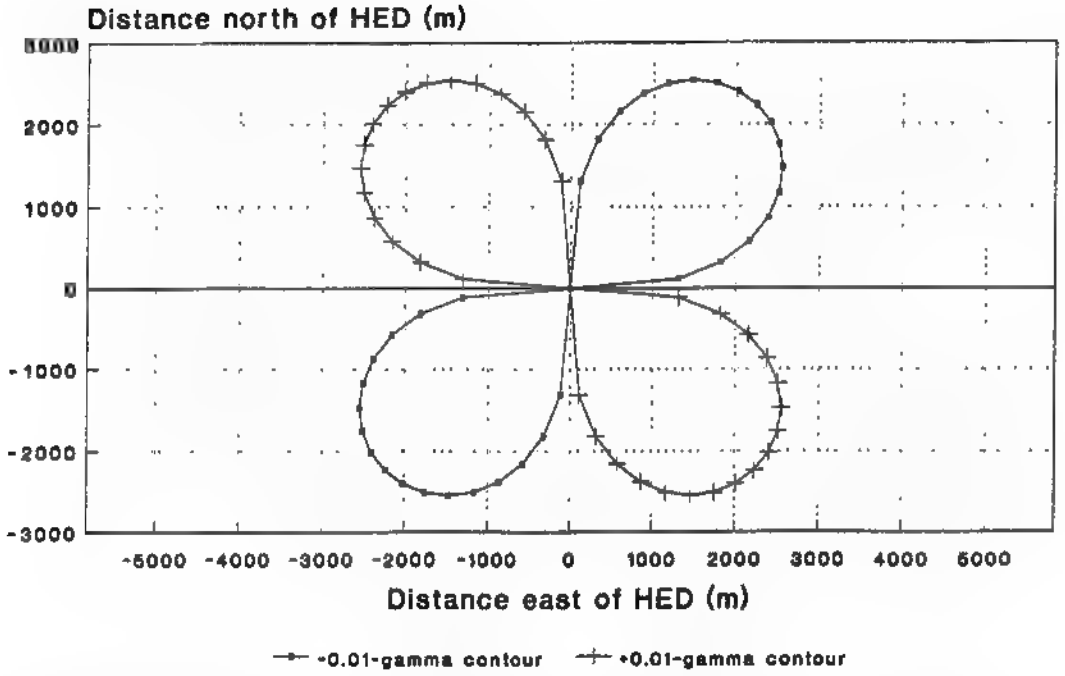

Figure 22. Horizontal sea-level slice of magnetic anomaly in submarine-fixed coordinates from a sea-surface static HED for earth's magnetic dip angle of 0° (magnetic equator).

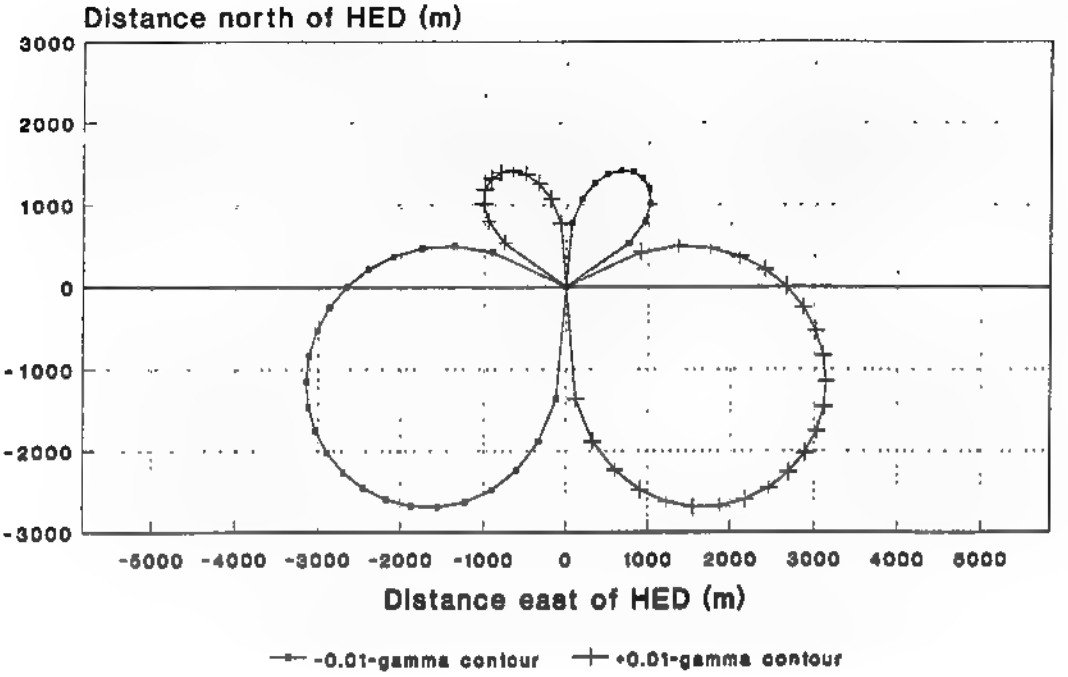

Figure 23. Horizontal sea-level slice of magnetic anomaly in submarine-fixed coordinates from a sea-surface static HED for earth's magnetic dip angle of 45° (mid-latitude).

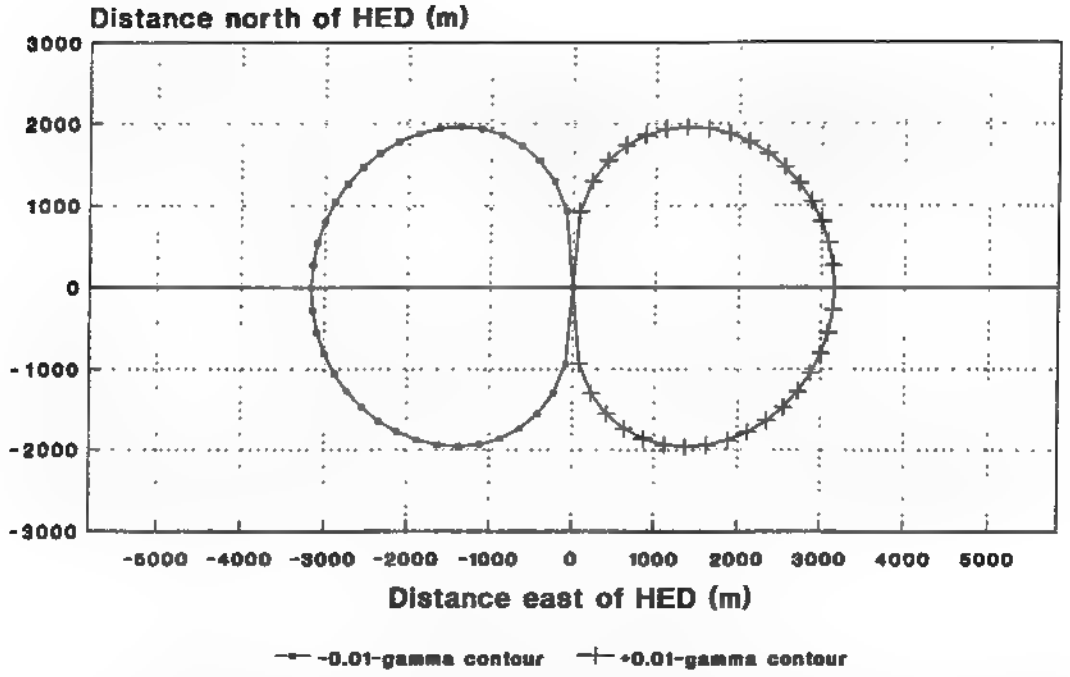

Figure 24. Horizontal sea-level slice of magnetic anomaly in submarine-fixed coordinates from a sea-surface static HED for earth's magnetic dip angle of 90° (north magnetic pole).

IV. MAGNETIC ANOMALY FROM THE ALTERNATING ELECTRIC CURRENT MOMENT OF A SUBMARINE

General

As indicated in Sections I and III, a submarine immersed in seawater behaves like a short-circuited galvanic cell which, because of variations in resistance (as a function of propeller shaft angle) between the rotating propeller shaft and its bearings, may produce an electric current that is modulated at the shaft rate. Equations for calculating the magnetic field intensity from a harmonic electric current dipole immersed in a semi-infinite conducting medium were taken from reference (c) and applied to the situation at hand in Appendix D.

If equations (D-10) through (D-15) for the alternating HED are compared to the corresponding equations (C-2) through (C-7) for the static HED, certain similarities and differences are observed. For example, an exponential attenuation factor appears in the equations for the alternating HED but not for the static HED. Also, the equations for the static HED tend to exhibit an inverse square law dependence of magnetic induction upon range whereas, for the alternating HED, the two horizontal components of magnetic induction tend to show an inverse cube law dependence upon range while the vertical component exhibits a generally inverse fourth power dependence upon range. If the equations for the special case of both the field point P and the HED being at the air-water interface are compared (i.e., (D-16) through (D-18) for the alternating HED compared with (C-8) through (C-10) for the static HED), the differences in range dependence can be seen more readily.

Equations (D-16) through (D-18) can be combined to yield an equation for calculating the magnetic anomaly Γ in a horizontal, sea-level plane from an alternating HED also at sea level:

$$\Gamma = [100\, p_s / (\gamma_1 \rho^3 B_E)] \{B_{Ex} [\sin(\phi + \theta) + \sin(\phi - \theta)] + B_{Ey} [\cos(\phi - \theta) - 3\cos(\phi + \theta)] + B_{Ez} [6 \sin\phi / (\gamma_1 \rho)]\}. \quad (23)$$

Note that, for this special case, at any given angle, Γ varies as $1/\rho^3$ for the contributions from the horizontal components and as $1/\rho^4$ for the contribution from the vertical component. Accordingly, equation (23) doesn't lend itself to an easy explicit solution for ρ as could be done with equation (22) for the case of the static HED. However, equation (23) permits the interesting observation that near the magnetic equator, where $B_{Ez} = 0$, Γ varies as $1/\rho^3$ while near the magnetic polar regions, B_{Ex} and B_{Ey} equal zero, and therefore Γ varies as $1/\rho^4$.

ELFE Profiles in Submarine-Fixed Coordinates

For a comparison of the magnetic anomalies from static and alternating HEDs, equations (22) and (23) are plotted in figure 25 on the same scale in polar form as a function of compass angle. The curves show the magnetic anomalies at sea level at a range of 1000 m

for static and alternating current moments $p_s = p_a = 1000$ A · m. Other assumed values are frequency f = 1 Hz, seawater conductivity $\sigma = 4$ S/m, and seawater dielectric constant k = 78, yielding a seawater propagation constant $\gamma_1 = 0.005619$ m^{-1}. The HEDs were assumed to be on a 000° magnetic heading at the sea surface at geographical coordinates 25°N, 58°E where the earth's dip angle is 37.8°. Note that at this range, the alternating anomaly has a structure similar to the static anomaly but which, at this range, is weaker despite the very large value assumed for p_a.

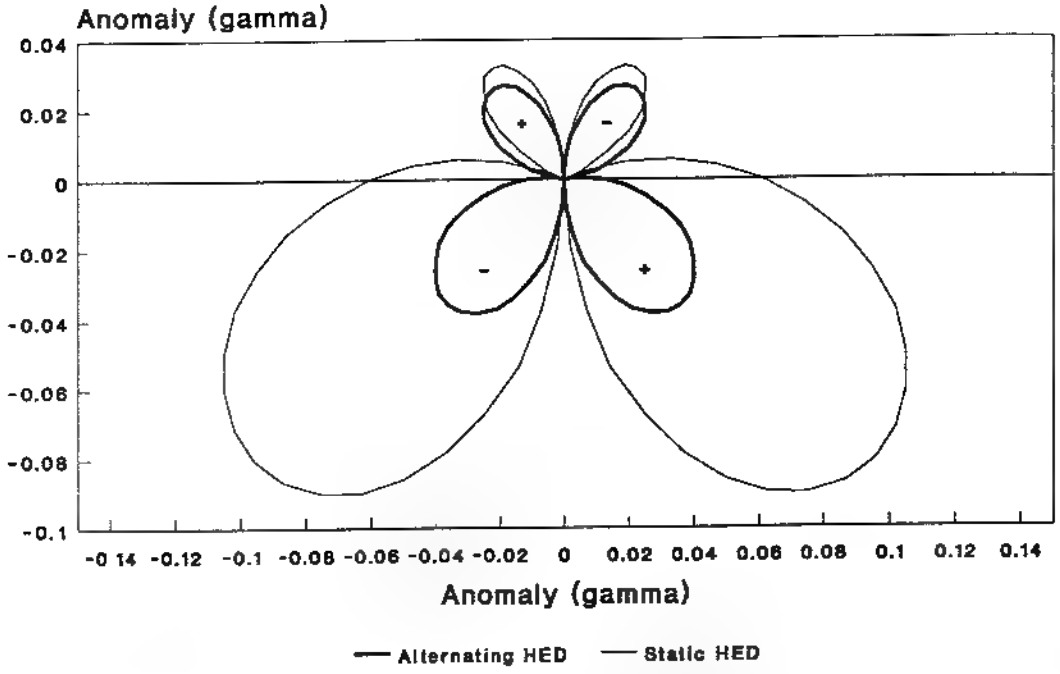

Figure 25. Cross plots of magnetic anomalies vs compass angle at 1000-m range at sea level for 1000-A · m static and alternating HEDs at the air-sea interface.

The orientation of an alternating HED anomaly varies as a function of HED heading in a way that is similar to that from a static HED. Figure 26 shows three polar plots of the magnetic anomaly at sea level as a function of compass angle at a constant range of 1000 m from a sea-level, 100-A · m, alternating HED for HED orientations of 000°, 045° and 090° true. A frequency of 4 Hz was assumed. The geographical coordinates were taken to be 25°N, 58°E. The dotted and dashed circles correspond to scale values of 0.001 and 0.002 gamma, respectively. The polarities shown for the lobes correspond to the situation at some instant in time at which the alternating component of the galvanic corrosion current in the submarine is directed from the stern toward the bow. During the next half cycle, the polarities would be reversed. If the sensor were to move rapidly from within, say, a positive lobe to a negative lobe, a sudden phase shift would be observed.

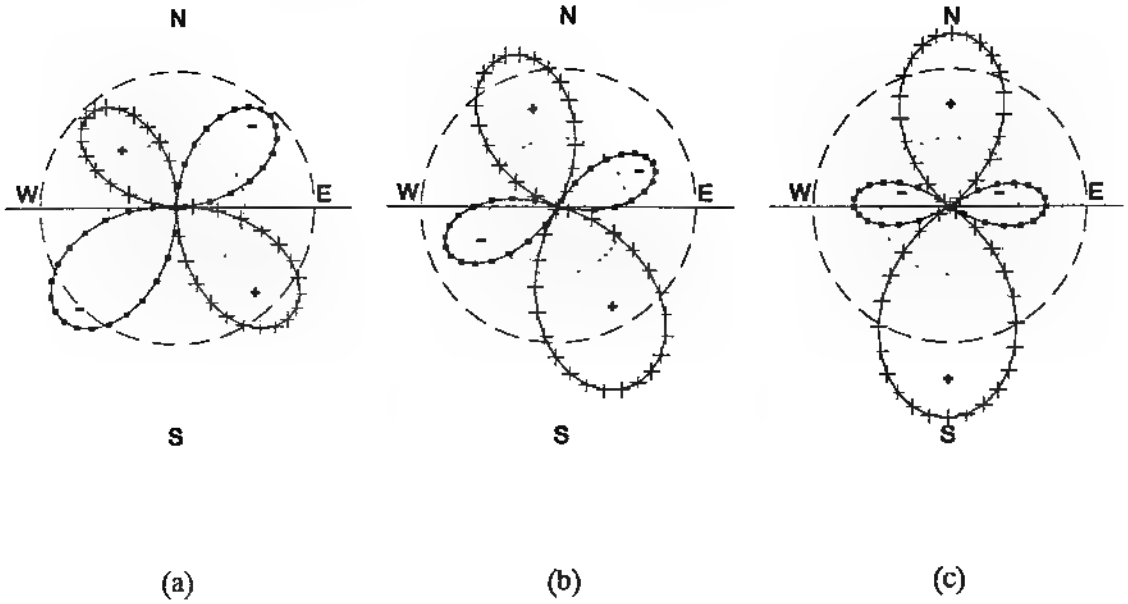

(a) (b) (c)

Figure 26. Polar plot of magnetic anomaly at a distance of 1000 m from an alternating 100-A · m HED vs compass angle, for three HED orientations: (a) 000°, (b) 045°, (c) 090°.

Figures 27 and 28 illustrate the structure in space of the magnetic anomaly from an alternating HED analogous to that shown in figures 18 and 19 for a static HED. Equations (D-10) through (D-15) and equations (C-11), (C-12), and (C-13) were used to produce these curves, which show the envelope, in HED coordinates, for which the anomaly equals +/– 0.001 gamma. The submarine was assumed to be at a depth of 30 m on a 090° magnetic heading at geographical coordinates 25°N, 58°E, where the earth's magnetic field dip angle is 37.8°. Its alternating electric current moment was assumed to be 100 A · m and to have a frequency of 4 Hz. Figure 27 shows the locus of points in a horizontal plane at sea level for which the anomaly is +0.001 γ for the lobes lying along the north-south axis and –0.001 γ for the lobes along the east-west axis. These polarities correspond to the instants in time at which the current within the submarine in the stern-to-bow direction is greater than the average dc value; these polarities reverse during each following half cycle. In figure 27, conditions 1 and 2 given in Appendix D for "Field point in air" are satisfied for ranges R>>89 m; thus values near the origin should be disregarded. Figure 28 shows vertical profiles, in three east-west planes, (a) 800 m south of the HED, (b) in the same plane as the HED, and (c) 800 m north of the HED. The solid portions of the curves in figure 28 represent values that satisfy all of the conditions given in Appendix D for both the above-water and below-water cases, whereas the dotted portions represent *terra incognita* for which the conditions are not satisfied resoundingly. It is seen that the underwater values appear valid only at the shallow depths farthest away from the HED. Because the equations used to calculate the underwater values assume that the energy propagates from the HED up to the surface, over a horizontal path, and down to the field point P, figure 28 underestimates the underwater ranges in the vicinity of the HED. Because the primary interest in this study is in investigating phenomena that will

yield detection ranges for airborne sensors that are longer than those currently achievable with conventional MAD, these shortcomings are not considered serious.

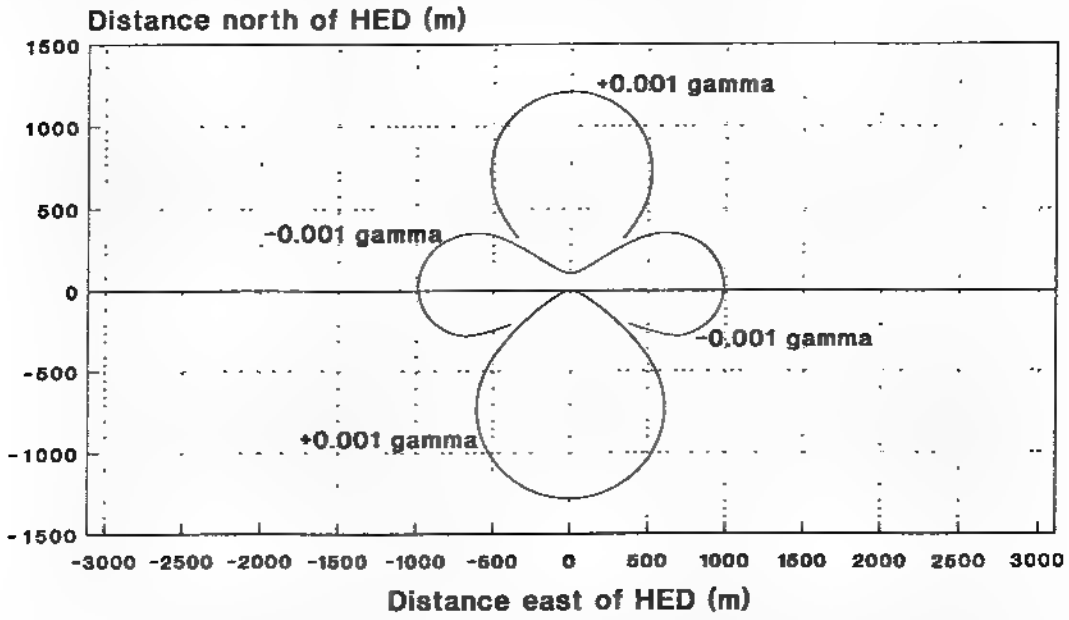

Figure 27. Sea-level horizontal section of magnetic anomaly from an alternating HED on 090° magnetic heading in submarine-fixed coordinates showing +/–0.001-γ contours.
HED: depth, 30 m; electric current moment, 100 A·m; frequency, 4 Hz.
Location: 25°N, 58°E. Earth's magnetic field dip angle: 37.8°.

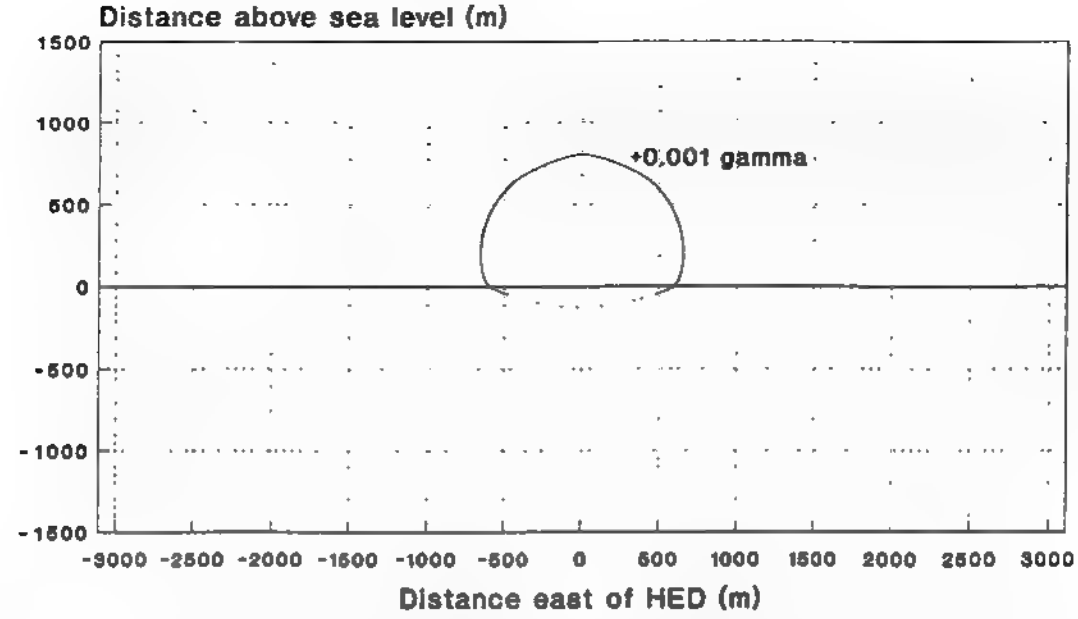

(a)

Figure 28. East-west vertical section of magnetic anomaly from an alternating HED on 090° magnetic heading in submarine-fixed coordinates showing +/–0.001-γ contours.
(a) 800 m south of HED
HED: depth, 30 m; electric current moment, 100 A·m; frequency, 4 Hz.
Location: 25°N, 58°E. Earth's magnetic field dip angle: 37.8°.

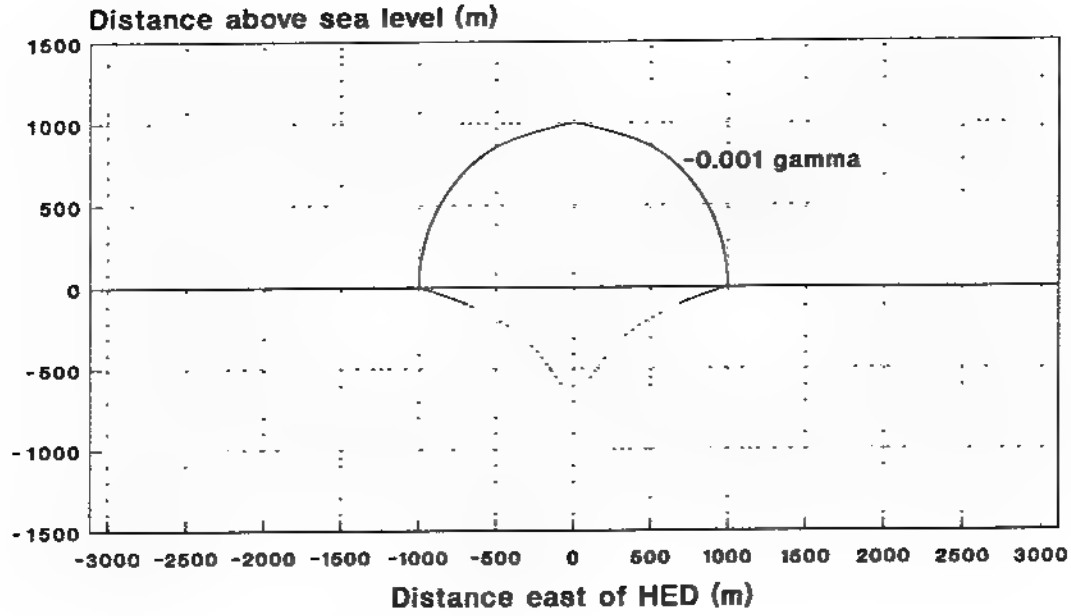

(b)

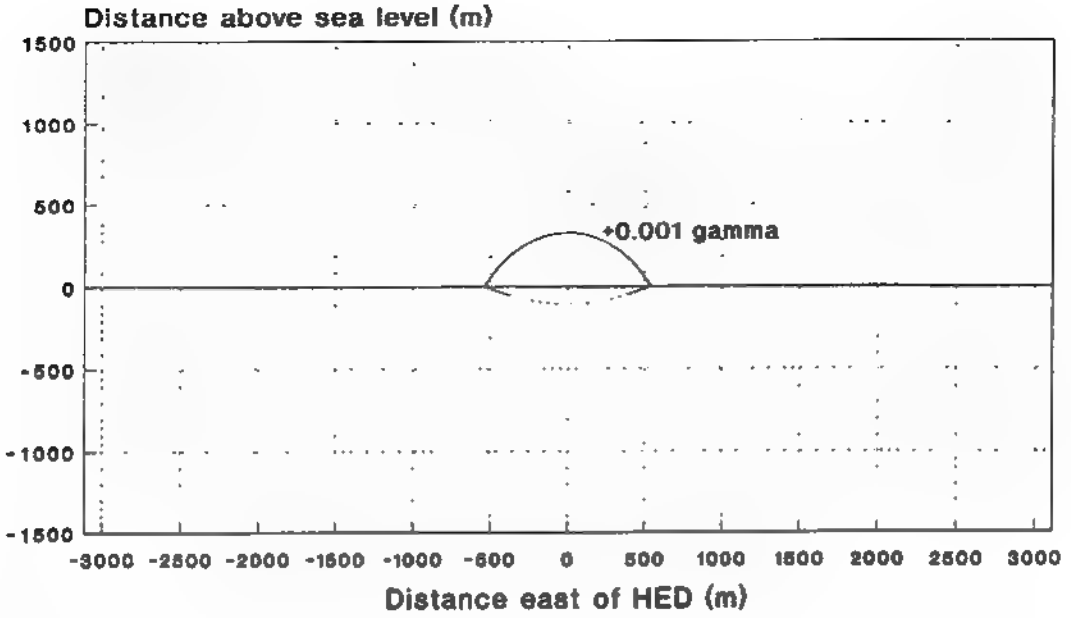

(c)

Figure 28. East-west vertical section of magnetic anomaly from an alternating HED on 090° magnetic heading in submarine-fixed coordinates showing +/–0.001-γ contours.
(b) 0 m north of HED (c) 800 m north of HED
HED: depth, 30 m; electric current moment, 100 A·m; frequency, 4 Hz.
Location: 25°N, 58°E. Earth's magnetic field dip angle: 37.8°.

If a scalar, total-field magnetometer of adequate sensitivity and response characteristics were to be flown on selected straight line paths through the alternating HED anomaly depicted in figures 27 and 28, the ELFE signals would exhibit envelopes such as shown in figures 29 and 30. Figure 29 is the envelope (or the motion-produced modulation) of the ELFE signal resulting from the movement of the aircraft past the HED on a north magnetic heading, 500 m east of the HED. The simulated sensor altitude is 50 m. Figure 29 may be considered as the amplitude profile of the anomaly along the "500-m east" grid line of figure 27. For ease in making the comparison, both figures have the same distance scales. In figure 29, two horizontal scale lines, calibrated at 50-m intervals, indicate where the curve crosses the +0.001- and –0.001-gamma levels, corresponding to the six intersections of the lobes of figure 27 with the "500-m east" grid line. (The agreement is not exact because figure 27 is a sea-level plot whereas the altitude for figure 29 is 50 m.)

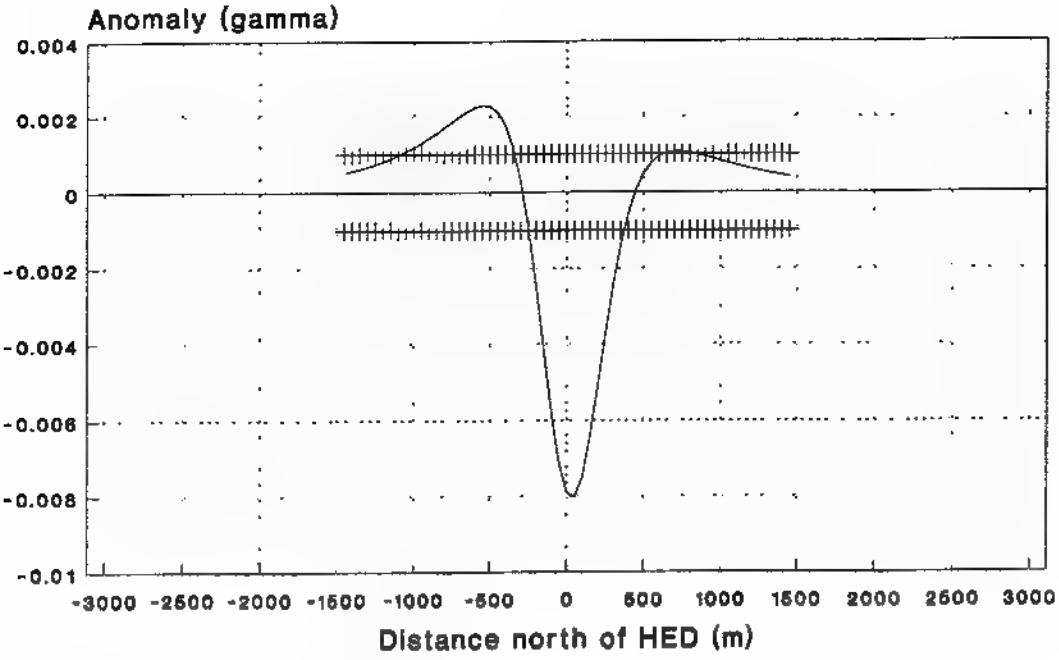

Figure 29. Envelope of magnetic anomaly in air from an alternating HED in seawater corresponding to a northerly sensor aircraft pass 500 m to the east of the HED.

Figure 30 is similar to figure 29 except the simulated sensor moves on an easterly heading, 800 m south of the HED and matches up with a cut through figure 28(a).

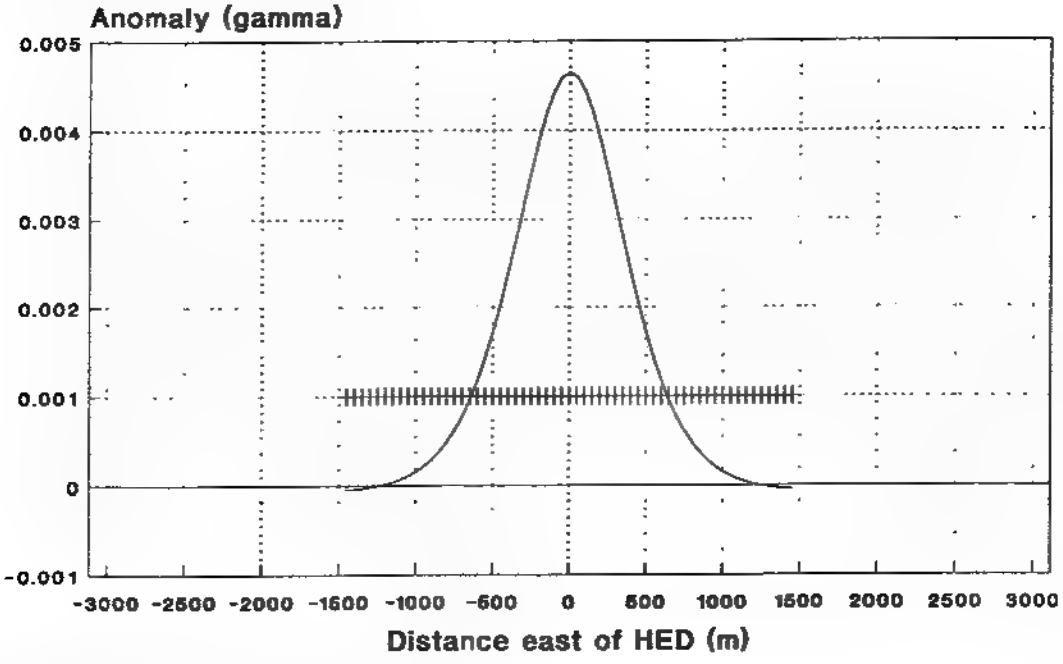

Figure 30. Envelope of magnetic anomaly in air from an alternating HED in seawater corresponding to an easterly sensor aircraft pass 800 m to the south of the HED.

Temporal Characteristics of ELFE Signatures

The ELFE signature appears to arise from abrupt, periodic, short-duration increases in electrical resistance between the propeller drive shaft and its hull-mounted bearings. Even if these changes in resistance are assumed to be instantaneous, the resulting changes in electric current will be smeared out in time because of the inductive and resistive properties of the system. Because the ELFE signals are "spikey," they will contain many frequencies that are harmonics of the shaft-rate fundamental. As the ELFE signal propagates through sea water, energy at the various frequencies propagates at different speeds, contributing to a further time-broadening of the pulses. In addition, attenuation in seawater is a function of frequency, causing further changes in the shape of received pulses. In the following paragraphs, an attempt is made to obtain a crude estimate of the shape of the received pulses.

The change Δi in electric current resulting from a small change ΔR in resistance in an electrical circuit of emf $\mathcal{E}$, resistance R, inductance L and inductive time constant $\tau_L = L/R$ as a function of time t is

$$\Delta i = - \mathcal{E} (t / RL + 1/R^2) \exp(-R\, t / L)\, \Delta R \qquad (24)$$

or approximately as

$$\Delta i \propto - \mathcal{E}\ \exp(-t / \tau_L)\, \Delta R. \qquad (25)$$

If it is assumed that the resistance R of the submarine-seawater circuit is about 0.03 Ω (consistent with an emf $\mathcal{E}$ = 1 V and a current i = 33 A) and the inductance L = 1 microhenry (consistent with a magnetic induction of 0.03 γ at a range of 250 m from a single-turn coil carrying a steady current of 33 A) the inductive time constant $\tau_L = L/R = 10^{-6}/0.03 = 33$ μs, which may be considered the intrinsic rise time of the ELFE pulse.

The speed of propagation of a plane electromagnetic wave of frequency f in seawater of conductivity 4 S/m is

$$v = 1600\ f^{1/2} \quad (m/s). \qquad (26)$$

If the depth (-h) of the alternating HED is 100 m and the ELFE fundamental frequency is 1 Hz, the transit time to the surface for the first ten harmonics will range from 19.8 ms to 62.5 ms, a spread of 42.7 ms.

The attenuation coefficient k for a plane electromagnetic wave in seawater of conductivity 4 S/m is

$$k = 0.004\ f^{1/2} \quad (m^{-1}) \qquad (27)$$

and the transmittance

$$\tau = \exp(k\,h) = \exp(0.004\,f^{1/2}\,h). \tag{28}$$

Thus, if h = −100 m, transmittances for the first ten harmonics (i.e., for 1 Hz ≤ f ≤ 10 Hz,) will range from 0.67 to 0.28. In accordance with equations (27) and (28), the lowest frequencies will suffer the least attenuation but, in accordance with equation (26), these lowest frequencies will incur the longest delays in propagating through the seawater. These lowest frequencies would also be expected to have the highest amplitudes.

The foregoing considerations were applied to calculate waveforms for ELFE pulses after they emerge from the sea for a fundamental frequency of 1 Hz and HED depths of 1, 10, 50, and 100 m. The initial waveform was assumed to have a very short duration and to have a sawtooth shape which could be represented by a Fourier series for which the initial relative amplitude of the n^{th} component was 1/n. Calculations were performed out to the thirtieth harmonic and the results are shown in figure 31. Widths of the four waveforms at their respective half-amplitude levels are 0.18 ms, 1.83 ms, 8.6 ms, and 16 ms for HED depths of 1 m, 10 m, 50 m, and 100 m.

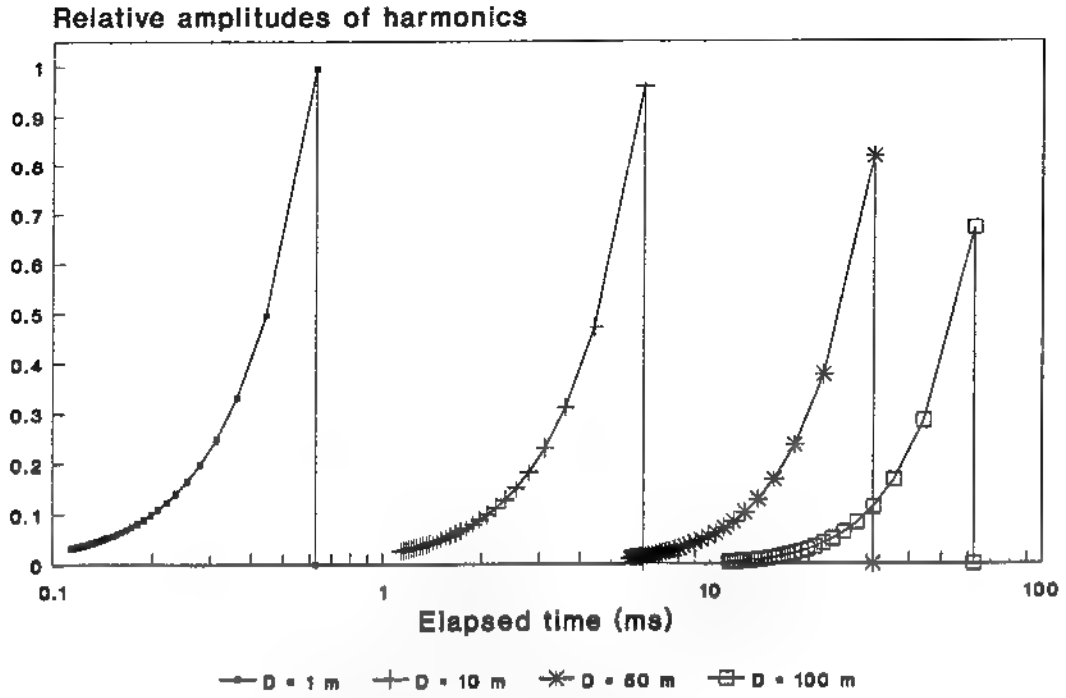

Figure 31. Calculated waveforms for ELFE pulses for alternating HED depths of 1 m, 10 m, 50 m, and 100 m.

If a sampling, scalar, total-field magnetometer is used to observe ELFE signatures it is important that (1) the duration of each sample be small compared to the duration of the ELFE pulse, and (2) an adequate number of samples be taken during each ELFE pulse. If the time per sample is too long, the signal will be diluted out over time. If the observation time per sample is appropriately short (i.e., much shorter than the ELFE pulse duration) but the

interval between samples is not small compared to the ELFE pulse duration, some pulses will be missed completely or only a small fraction of the individual pulses will be detected.

The AN/ASQ-208 takes 432 samples per second; the time interval between successive samples is, therefore, 2.31 ms. For an HED depth of 100 m, the received ELFE half-amplitude pulse duration is shown in figure 31 to be 16 ms; therefore, on average, a probably adequate 6.9 samples would be taken per pulse. For the shallower depths, on the other hand, the duration of the pulses may be shorter than the time interval between samples. Consequently, many of these short duration pulses could be sampled inadequately or even missed completely. It appears that if ELFE pulses from alternating HEDs as shallow as 10 m are to be sampled at a rate of at least two per pulse, the interval between samples should be reduced to 1.83/2 ms, corresponding to 1093 samples per second.

Figure 32 illustrates the signature that an ideal, scalar, total-field magnetometer would produce upon passing on an easterly heading 800 m to the south of a 30-m deep, 4-Hz, alternating HED on a 090° magnetic heading. (The envelope of this signature appears in figure 30 on a scale of distance rather than time.)

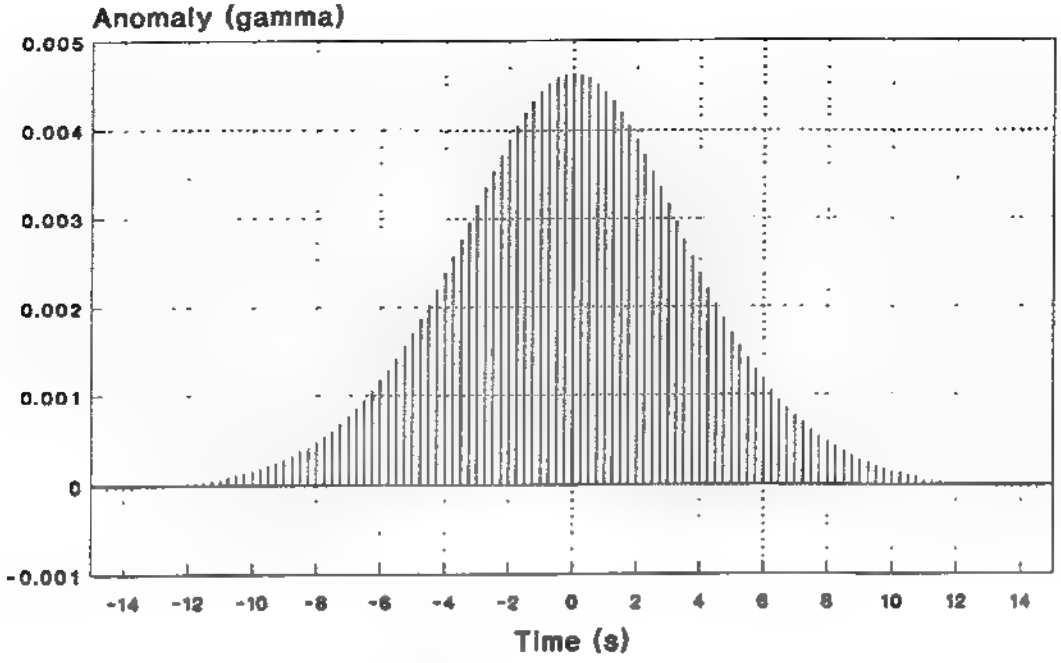

Figure 32. Magnetic anomaly in air from an alternating HED in seawater corresponding to an easterly sensor aircraft pass 800 m to the south of the HED.

V. COMBINATION OF FERROMAGNETIC, STATIC HED, AND ALTERNATING HED ANOMALIES

In the foregoing sections, each of the types of anomalies was treated separately. Because each anomaly is simply the projection of magnetic induction vectors onto the earth's magnetic induction vectors, the anomalies at any point can be combined by algebraic addition. Figure 33 shows anomaly signatures for a ferromagnetic dipole, a static HED, an alternating HED, and the combination of the three. The target was assumed to be a 7600-ton submarine operating at a depth of 30 m on a 270° magnetic heading at coordinates 25°N, 58°E. Its static electric current moment was assumed to be 1000 A · m, directed from the stern toward the bow. The alternating electric current moment was taken as 100 A · m from stern to bow and to have a frequency of 4 Hz. The sensor aircraft was assumed to be flying at a speed of 100 m/s, on a course of 090° magnetic, at an altitude of 50 m, 800 m to the south of the target.

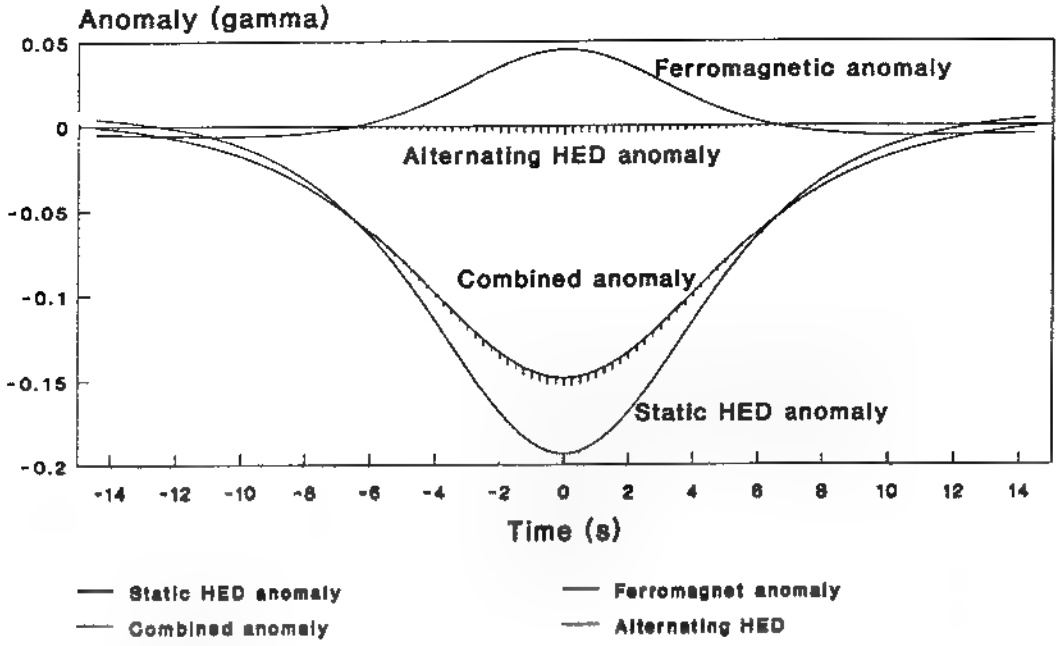

Figure 33. Anomaly signatures for a ferromagnetic dipole, a static HED, an alternating HED, and the combination of the three. See text for assumptions.

This particular combination of parameters was chosen to enable each of the effects to be seen on the same chart. For example, the point of closest approach to the target was 800 m, which is beyond typical current MAD range. At significantly shorter ranges, the ferromagnetic dipole anomaly would have swamped the HED anomalies. The westerly

heading was chosen for the submarine so that the static HED anomaly would partially cancel the ferromagnetic anomaly, thus increasing the relative magnitude of the alternating HED anomaly. For the assumed conditions, the magnitude of the static HED anomaly exceeds that of the ferromagnetic anomaly. This occurs, in part, because the ferromagnetic anomaly decreases as the cube of distance whereas the static HED anomaly decreases as the square of distance. Obviously, many other combinations are possible.

The particular aircraft path assumed for figure 33 was chosen to keep the frequency components of the ferromagnetic signal low in comparison to the alternating HED frequency to enable easy separation of the latter from the former by simple high-pass filtering. If, for example, the aircraft had flown at low altitude directly over the submarine, with both on 000° headings, the higher harmonics of the ferromagnetic signal would seriously compete with the 4-Hz alternating HED signal and probably render it undetectable.

A convenient rule of thumb for estimating the fundamental frequency f_0 of the ferromagnetic anomaly can be inferred by referring to figure 5 and noting that if the sensor were to move in a circular path in the plane of the figure at speed v at a distance R from the origin, it would sense two cycles of change in the magnetic field per 360° of rotation. Thus

$$f_0 \approx v/(\pi R) \quad \text{(Hz)}. \tag{29}$$

To illustrate equation (29), consider a case in which the sensor aircraft were to pass on a northerly course at a speed of 100 m/s and an altitude of 50 m over a 30-m deep submarine. The fundamental frequency f_0 of the ferromagnetic anomaly directly over the submarine would be 0.4 Hz, which, with its harmonics, approximates the ELFE frequencies associated with the propeller rotation rate. The magnitude of the ferromagnetic signal would be many tens of gamma and thus would be extremely difficult, if not impossible, to separate from the ELFE signal.

VI. DISCUSSION

For current generation submarines and current generation MAD sensors in fixed-wing aircraft, the dominant signature arises from the ferromagnetic moment of the submarine. The anomaly from the static electric current moment serves to introduce small distortions of the ferromagnetic signature; the anomaly from the alternating component of the electric current moment is essentially undetectable, largely because of competition from the ferromagnetic anomaly. Both the ferromagnetic and alternating HED anomalies drop off largely with the cube of the range, whereas the anomaly from the static HED drops off as the square of the range.

If MAD sensors of significantly improved usable sensitivity can be developed and competing noise can be driven down, detection ranges may improve to the point where the static HED anomaly dominates. At these longer ranges, the ferromagnetic anomaly and the alternating HED anomaly will have dropped off in the same proportion; however, because the HED frequency is independent of aircraft location but the frequency of the ferromagnetic anomaly varies inversely as range, it may be posible to separate the two signatures at the longer ranges. Detection of the alternating HED signature would provide information on the submarine's state of motion that the other signatures do not provide.

Use of the static HED signature (at the longer ranges achievable at higher sensitivities) could provide information on the heading of the target submarine that is not generally (and unambiguously) available from the ferromagnetic signature.

Useful detection of ELFE signals by a scalar, total-field magnetometer in a fixed-wing aircraft appears improbable as compared to detection of a passing submarine by a fixed-site sensor. Fixed-site sensors offer the relative advantages of freedom from platform and geological noise, much longer integration times, the ability to exploit the vector nature of the signature, and a much larger separation in frequency between the ELFE signal and the ferromagnetic signal.

VII. ACKNOWLEDGEMENT

The author acknowledges the contributions of Dr. Stephen P. Haimbach and Mr. Mark Hryszko, Pacific-Sierra Research Corporation, in generating the three-dimensional images of the anomaly produced in the earth's magnetic field by a point ferromagnetic dipole.

VIII. REFERENCES

(a) P. M. Moser, *Magnetic Signatures of Submarines I*, Pacific-Sierra Research Corporation, PSR Report 2474, June 1994.

(b) E. I. Peizer, *Magnetic Moments and Fields of Submarines (U)*, Naval Ordnance Laboratory *MAGNETIC ANOMALY DETECTOR (MAD) SYMPOSIUM*, NOLTR 72-49, D. F. Bleil, Editor, CONFIDENTIAL, 1 March 1972.

(c) M. B. Kraichman, *Handbook of Electromagnetic Propagation in Conducting Media*, Second Printing, U. S. Government Printing Office, Stock No. 008-040-00074-5, 1976.

APPENDIX A

MAGNETIC ANOMALY FROM A POINT FERROMAGNETIC DIPOLE

The magnetic induction **B** produced at a field point P by a point ferromagnetic dipole is given in vector notation by the following expression

$$\mathbf{B} = -\mathbf{M}/R^3 + 3(\mathbf{M}\cdot\mathbf{R})\,\mathbf{R}/R^5 \qquad \text{(A-1)}$$

in which **M** is the magnetic moment vector of the dipole,

R is a range vector extending from the dipole to point P, and

R is the magnitude of **R**.

Let P(x,y,z) = field point at which anomaly Γ is to be calculated

h = elevation of dipole relative to sea level (–depth) (ft)

$x = R_x$ = distance of P east of dipole (ft)

$y = R_y$ = distance of P north of dipole (ft)

$z = R_z + h$ = distance of P above sea level (ft)

B_x = easterly component of magnetic induction from dipole (γ)

B_y = northerly component of magnetic induction from dipole (γ)

B_z = vertically upward component of magnetic induction from dipole (γ)

B_{Ex} = easterly component of earth's magnetic induction (nT or γ)

B_{Ey} = northerly component of earth's magnetic induction (nT or γ)

B_{Ez} = vertically upward component of earth's magnetic induction (nT or γ)

B_E = magnitude of the earth's magnetic induction vector at P (nT or γ)

$R = [x^2 + y^2 + (z - h)^2]^{1/2}$

$B_E = (B_{Ex}^2 + B_{Ey}^2 + B_{Ez}^2)^{1/2}$ (nT or γ)

Each of the vectors in equation (A-1) can be resolved into easterly (x), northerly (y), and vertically upward (z) components as follows:

$$\mathbf{B} = \mathbf{i}\, B_x + \mathbf{j}\, B_y + \mathbf{k}\, B_z \tag{A-2}$$

$$\mathbf{M} = \mathbf{i}\, M_x + \mathbf{j}\, M_y + \mathbf{k}\, M_z \tag{A-3}$$

$$\mathbf{R} = \mathbf{i}\, R_x + \mathbf{j}\, R_y + \mathbf{k}\, R_z = \mathbf{i}\, x + \mathbf{j}\, y + \mathbf{k}\,(z - h) \tag{A-4}$$

Substituting equations (A-2), (A-3), and (A-4) into equation (A-1) yields

$$\mathbf{i}\, B_x + \mathbf{j}\, B_y + \mathbf{k}\, B_z = -(\mathbf{i}\, M_x + \mathbf{j}\, M_y + \mathbf{k}\, M_z) / R^3$$

$$+ 3\,(M_x R_x + M_y R_y + M_z R_z)(\mathbf{i}\, R_x + \mathbf{j}\, R_y + \mathbf{k}\, R_z) / R^5. \tag{A-5}$$

Collecting terms along each of the axes yields

$$\mathbf{i}\, B_x = -\mathbf{i}\, M_x / R^3 + 3\,(M_x R_x + M_y R_y + M_z R_z)\, \mathbf{i}\, R_x / R^5 \tag{A-6}$$

$$\mathbf{j}\, B_y = -\mathbf{j}\, M_y / R^3 + 3\,(M_x R_x + M_y R_y + M_z R_z)\, \mathbf{j}\, R_y / R^5 \tag{A-7}$$

$$\mathbf{k}\, B_z = -\mathbf{k}\, M_z / R^3 + 3\,(M_x R_x + M_y R_y + M_z R_z)\, \mathbf{k}\, R_z / R^5. \tag{A-8}$$

Therefore, the magnitudes of the east, north, and upward components are, respectively,

$$B_x = 3\,[M_x x + M_y y + M_z (z - h)]\, x / R^5 - M_x / R^3 \tag{A-9}$$

$$B_y = 3\,[M_x x + M_y y + M_z (z - h)]\, y / R^5 - M_y / R^3 \tag{A-10}$$

$$B_z = 3\,[M_x x + M_y y + M_z (z - h)]\,(z - h) / R^5 - M_z / R^3. \tag{A-11}$$

The anomaly Γ at point P can then be calculated from

$$\Gamma = (B_x B_{Ex} + B_y B_{Ey} + B_z B_{ez}) / B_E \quad (\gamma). \tag{A-12}$$

APPENDIX B

SEQUENCE OF STEREO PAIR REPRESENTATIONS OF ANOMALY FROM A POINT FERROMAGNETIC DIPOLE

Thirty-six different (of a total of 40) horizontal views of the anomaly from a point ferromagnetic dipole in submarine-fixed coordinates illustrated in figure 4 are shown in figure B-1. The angle at which the first image is viewed is toward the east at 095° (magnetic) and successive images are viewed at 10-degree angular increments, proceeding around the compass in a counterclockwise manner. Thus, in the first row, the viewing angles are 095°, 085°, 075°, 065°, 055°, 045°, 035°, 025°, 015°, and 005°. The image at the end of each row is repeated at the beginning of the next row. Therefore, in the second row, the viewing angles are 005°, 355°, 345°, . . . 275°. The ranges of angles for the third and fourth rows are 275° . . . 185°, and 185° . . . 95°, respectively. The images are arranged such that they can be viewed as a succession of stereo pairs.

The submarine was assumed to be on a north magnetic heading in the Strait of Hormuz where the inclination of the earth's magnetic field is 40.3° (downward). The submarine was assumed to behave as a point ferromagnetic dipole having a resultant moment of $4.39 \times 10^7\ \gamma \cdot m^3$ ($15.5 \times 10^8\ \gamma \cdot ft^3$) inclined downward at an angle of 27.2°. The axis of highest symmetry of the anomaly lies in the plane defined by the earth's field vector and the magnetic moment vector of the submarine (in this case, a vertical plane) and it bisects the angle formed by these two vectors; i.e., its depression angle is 33.75°.

The toroid-shaped portion of the anomaly has, from equation (15), an outer radius of 1140 m (3741 ft) and its surface is the locus of points for which the anomaly has a value of $-0.03\ \gamma$. Similarly, from equation (14), the maximum radial extent of the dumbbell-shaped portion of the anomaly is 1427 m (4682 ft) and its surface is the locus of points for which the anomaly has a value of $+0.03\ \gamma$.

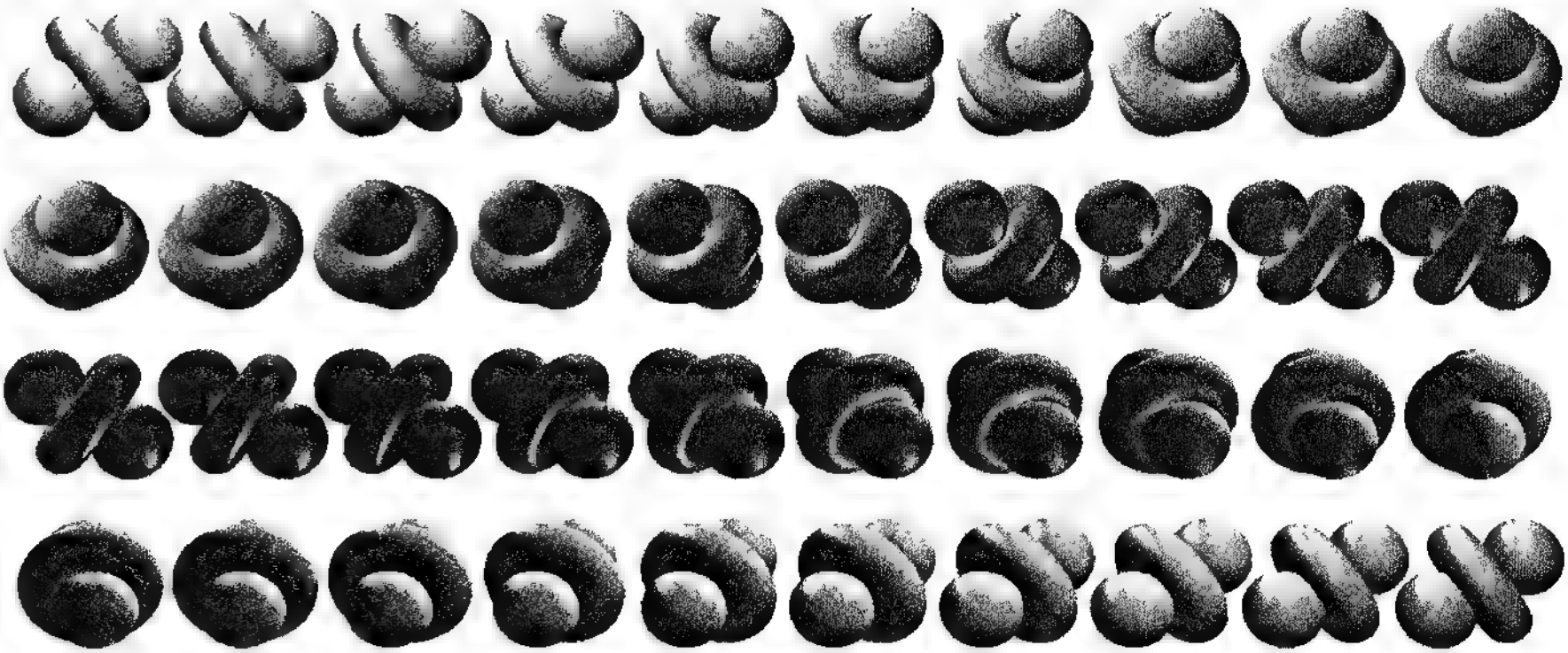

Figure B-1. Sequence of stereo pair images of a magnetic anomaly in submarine-fixed coordinates viewed from 36 directions in the horizontal plane.

APPENDIX C

MAGNETIC ANOMALY ABOVE AND BELOW THE AIR-SEA INTERFACE FROM A STATIC HORIZONTAL ELECTRIC CURRENT ELEMENT IN SEAWATER

Kraichman (reference (c)) provides equations that enable one to calculate the magnetic field intensity **H** (in amperes/meter) in each of two semi-infinite media (e.g., atmosphere and sea) from a horizontal electric current dipole (HED) in the lower medium positioned on the z-axis at an elevation h relative to the interface, parallel to the x-axis and positively directed. (Note that h requires a negative sign for an immersed source.) See figure C-1.

$$H_{\rho_2} = \frac{-p \sin\phi}{4\pi}\left[\frac{z-h}{R_1^3} + \left(\frac{\sigma_1-\sigma_2}{\sigma_1+\sigma_2}\right)\frac{1}{\rho^2}\left(\frac{z-h}{R_1}-1\right)\right]$$

$$H_{\phi_2} = \frac{-p \cos\phi}{4\pi}\left[\frac{z-h}{R_1^3} - \left(\frac{\sigma_1-\sigma_2}{\sigma_1+\sigma_2}\right)\frac{z-h}{R_1^3} - \left(\frac{\sigma_1-\sigma_2}{\sigma_1+\sigma_2}\right)\frac{1}{\rho^2}\left(\frac{z-h}{R_1}-1\right)\right]$$

$$H_{z_2} = \frac{p \sin\phi}{4\pi}\left(\frac{\rho}{R_1^3}\right)$$

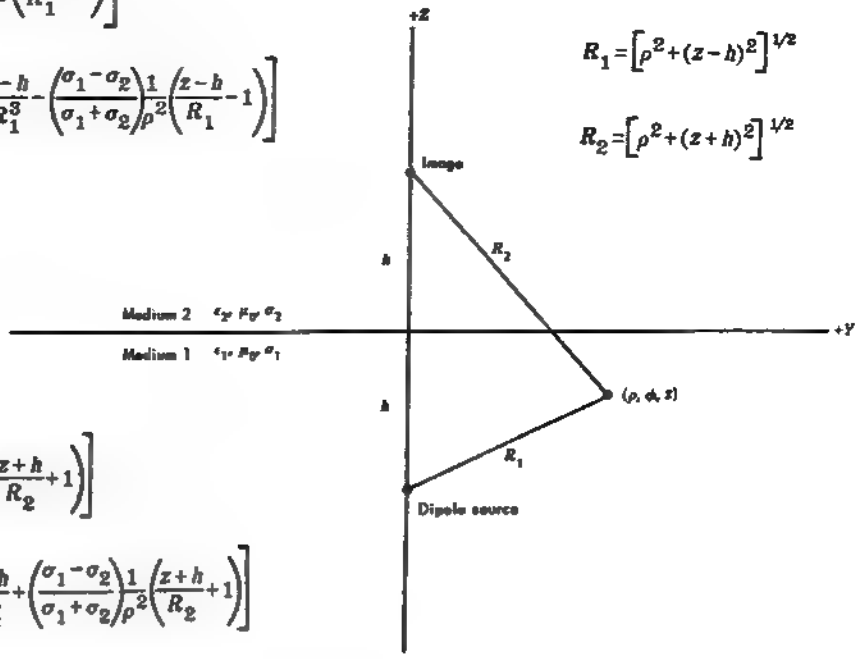

$$R_1 = \left[\rho^2 + (z-h)^2\right]^{1/2}$$

$$R_2 = \left[\rho^2 + (z+h)^2\right]^{1/2}$$

$$H_{\rho_1} = \frac{-p \sin\phi}{4\pi}\left[\frac{z-h}{R_1^3} - \left(\frac{\sigma_1-\sigma_2}{\sigma_1+\sigma_2}\right)\frac{1}{\rho^2}\left(\frac{z+h}{R_2}+1\right)\right]$$

$$H_{\phi_1} = \frac{-p \cos\phi}{4\pi}\left[\frac{z-h}{R_1^3} + \left(\frac{\sigma_1-\sigma_2}{\sigma_1+\sigma_2}\right)\frac{z+h}{R_2^3} + \left(\frac{\sigma_1-\sigma_2}{\sigma_1+\sigma_2}\right)\frac{1}{\rho^2}\left(\frac{z+h}{R_2}+1\right)\right]$$

$$H_{z_1} = \frac{p \sin\phi}{4\pi}\left(\frac{\rho}{R_1^3}\right)$$

Figure C-1. Geometry and equations for the magnetic field intensity above and within a semi-infinite conducting medium in which a static horizontal electric current dipole is immersed (from Kraichman, 1976).

Kraichman defines two distance parameters R_1 and R_2 in cylindrical coordinates as the distances to a field point $P(\rho, \phi, z)$ from, respectively, the current element in the lower medium and its image directly above it in the upper medium. Figure C-1 illustrates the geometry and gives Kraichman's equations for three orthogonal components of the magnetic field intensity in the lower medium (medium 1) and the upper medium (medium 2). Note that the equations for the vertical component H_z are identical for both media but differences in signs occur in the equations for the other two components. The steady electric current moment p_s is the product of the steady effective current I_s and the effective length L, i.e., $p_s = I_s L$. The electrical conductivities of medium 1 and medium 2 are σ_1 and σ_2, respectively. If the earth's atmosphere is taken as medium 2, its conductivity may be taken as zero; this assumption causes all of the factors involving σ_1 and σ_2 to vanish.

In the absence of magnetic materials at field point P, one can convert magnetic field intensity H (in A/m) to magnetic induction B (in nanotesla or gamma) as follows:

$$1 \text{ A/m} = 4\pi \times 10^{-7} \text{ T} = 400\pi \text{ nT} = 400\pi \text{ gamma}. \qquad \text{(C-1)}$$

Thus, the equations of figure C-1 can be recast to yield the magnetic induction at field point P as follows.

Case I. $z \leq 0$ (P in seawater)

$$B_{\rho 1} = -100\, p_s \sin\phi \,\{(z-h)/R_1^3 - [(z+h)/R_2 + 1]/\rho^2\} \qquad \text{(C-2)}$$

$$B_{\phi 1} = -100\, p_s \cos\phi \,\{(z-h)/R_1^3 + (z+h)/R_2^3 + [(z+h)/R_2 + 1]/\rho^2\} \qquad \text{(C-3)}$$

$$B_{z1} = 100\, p_s \sin\phi \;\; \rho/R_1^3 \qquad \text{(C-4)}$$

Case II. $z \geq 0$ (P in air)

$$B_{\rho 2} = -100\, p_s \sin\phi \,\{(z-h)/R_1^3 + [(z-h)/R_1 - 1]/\rho^2\} \qquad \text{(C-5)}$$

$$B_{\phi 2} = 100\, p_s \cos\phi \;\; [(z-h)/R_1 - 1]/\rho^2 \qquad \text{(C-6)}$$

$$B_{z2} = 100\, p_s \sin\phi \;\; \rho/R_1^3 \qquad \text{(C-7)}$$

Case III. $z = 0$ and $h = 0$ (Both field point P and HED at air-water interface)

$$B_{\rho 1} = B_{\rho 2} = B_\rho = 100\, p_s \sin\phi / \rho^2 \qquad \text{(C-8)}$$

$$B_{\phi 1} = B_{\phi 2} = B_\phi = -100\, p_s \cos\phi / \rho^2 \qquad \text{(C-9)}$$

$$B_{z1} = B_{z2} = B_z = 100\, p_s \sin\phi / \rho^2 \qquad \text{(C-10)}$$

For calculating the magnetic anomaly, it is convenient to convert to Cartesian coordinates and then to compass coordinates.

Let $P(x,y,z)$ = field point at which anomaly Γ is to be calculated

x = distance east of HED (m)

y = distance north of HED (m)

z = distance above sea level (m)

B_x = easterly component of magnetic induction from HED (γ)

B_y = northerly component of magnetic induction from HED (γ)

B_z = vertically upward component of magnetic induction from HED (γ)

B_{Ex} = easterly component of earth's magnetic induction (nT or γ)

B_{Ey} = northerly component of earth's magnetic induction (nT or γ)

B_{Ez} = vertically upward component of earth's magnetic induction (nT or γ)

B_E = magnitude of the earth's magnetic induction vector at P (nT or γ)

α = HED compass direction (degrees true)

$\rho = (x^2 + y^2)^{1/2}$ (m)

θ = arctan y/x (degrees)

$\phi = \alpha + \theta - 90$ (degrees)

$B_E = (B_{Ex}^2 + B_{Ey}^2 + B_{Ez}^2)^{1/2}$ (nT or γ)

For either Case I, Case II, or Case III

$$B_x = B_\rho \cos\theta - B_\phi \sin\theta \quad (\gamma), \tag{C-11}$$

$$B_y = B_\rho \sin\theta + B_\phi \cos\theta \quad (\gamma) \quad \text{and} \tag{C-12}$$

$$\Gamma = (B_x B_{Ex} + B_y B_{Ey} + B_z B_{ez}) / B_E \quad (\gamma) \tag{C-13}$$

APPENDIX D

MAGNETIC ANOMALY ABOVE AND BELOW THE AIR-SEA INTERFACE FROM AN ALTERNATING HORIZONTAL ELECTRIC CURRENT ELEMENT IN SEAWATER

Kraichman (reference (c)) provides equations that enable one to calculate the magnetic field intensity **H** (in amperes/meter) in each of two semi-infinite media (e.g., atmosphere and sea) from a horizontal electric current dipole (HED) in the lower medium positioned on the z-axis at an elevation h relative to the interface, parallel to the x-axis and positively directed. (Note that h requires a negative sign for an immersed source.) See figure D-1 and the drawing of figure C-1. The distance parameter R is defined in cylindrical coordinates as the distance to a field point P(ρ, ϕ, z) from a point on the air-sea interface directly over the alternating HED.

Subsurface to free-space propagation formulas for the quasi-static range, with $|\gamma_1 R| \gg 1$ *and* $R \gg |h|$

Dipole type	H_ρ	H_ϕ	H_z
HED	$\frac{p \sin\phi}{2\pi\gamma_1}\frac{e^{\gamma_1 h}}{R^3}\left[2-\frac{3z^2}{R^2}\right]$	$-\frac{p\cos\phi}{2\pi\gamma_1}\frac{e^{\gamma_1 h}}{R^3}$	$\frac{3p\sin\phi}{2\pi\gamma_1^2}\frac{\rho e^{\gamma_1 h}}{R^5}\left[1+\gamma_1 z-\frac{5z^2}{R^2}\right]$

(a)

Subsurface to subsurface propagation formulas for the quasi-static range, when $|\gamma_0\rho| \ll 1 \ll |\gamma_1\rho|$ *with* $\rho \gg |h|$ *and* $|z|$

Dipole type	H_ρ	H_ϕ	H_z
HED	$\frac{p\sin\phi}{\pi\gamma_1\rho^3}e^{\gamma_1(h+z)}$	$-\frac{p\cos\phi}{2\pi\gamma_1\rho^3}e^{\gamma_1(h+z)}$	$\frac{3p\sin\phi}{2\pi\gamma_1^2\rho^4}e^{\gamma_1(h+z)}$

(b)

Figure D-1. Equations for (a) subsurface-to-free-space propagation and (b) subsurface-to-subsurface propagation for the quasi-static range (from Kraichman, 1976).

The symbols used in figure D-1 are the same as those used in Appendix C except

$p = p_s$ = the alternating electric current moment

$R = (\rho^2 + z^2)^{1/2}$ = distance to a field point P(ρ, ϕ, z) from a point on the air-sea interface directly over the alternating HED

γ_0 = propagation constant for free space (air)

γ_1 = propagation constant for a homogeneous conducting half-space (seawater).

Kraichman gives the propagation constant γ through the expression

$$\gamma^2 = -\omega^2 \mu \varepsilon + j \omega \mu \sigma \qquad \text{(D-1)}$$

in which ω = the angular frequency of the source = $2 \pi f$

μ = the magnetic permeability constant of the medium

ε = the electrical permittivity constant of the medium

$j = (-1)^{1/2}$

σ = the electrical conductivity of the medium.

For air or seawater, $\mu = \mu_0 = 4 \pi \times 10^{-7}$ T · m/A. In air, $\varepsilon = \varepsilon_0 = 8.85 \times 10^{-12}$ $C^2/N \cdot m^2$; in seawater, $\varepsilon = 78\ \varepsilon_0$. For air, $\sigma = \sigma_2 = 0$ and, for seawater, $\sigma = \sigma_1 = 4$ S/m. In the following discussion of the conditions under which the equations listed in figure D-1 are valid it is assumed that the frequencies of interest are less than 100 Hz.

Field Point P in Air

Condition 1. $|\gamma_1 R| >> 1$

For frequencies of interest, it can be shown that the first term on the right side of equation (D-1) is many orders of magnitude smaller than the second term and, therefore, negligible in comparison. Thus, the modulus

$$|\gamma_1| = (\omega \mu \sigma)^{1/2} = (2 \pi f \mu_0 \sigma)^{1/2} = 5.620 \times 10^{-3} f^{1/2} \quad \text{or} \qquad \text{(D-2)}$$

$$5.620 \times 10^{-3} f^{1/2} R >> 1. \qquad \text{(D-3)}$$

It follows that the range R must therefore satisfy the condition

$$R >> 177.9/f^{1/2}. \qquad \text{(D-4)}$$

If the symbol ">>" is interpreted as meaning "ten times greater" then the range R must exceed $1779/f^{1/2}$. Thus, for f = 1 Hz, R must exceed 1779 m and, for f = 4 Hz, R must exceed 890 m.

Condition 2. $R >> |h|$

If, for example, the depth of the HED is 100 m, the equations are valid for ranges R greater than 1000 m, if the above interpretation of ">>" is held. Because R is reckoned from the sea surface (rather than from the HED), it is actually possible for R to be less than the depth |h| of the HED. Thus, care must be exercised to insure that, when calculations are performed for P nearly or directly over the HED, the altitude of P is much larger than the depth of the HED.

Field Point P in Seawater

Condition 1. $|\gamma_0 \rho| << 1$

Because the conductivity of air $\sigma = \sigma_2 = 0$, the second term of equation (D-1) vanishes when the modulus $|\gamma_0|$ of the propagation constant in air is calculated. Thus,

$$|\gamma_0| = \omega(\mu_0 \varepsilon_0)^{1/2} = 2 \pi f (\mu_0 \varepsilon_0)^{1/2} = 2 \pi f / c = 2.096 \times 10^{-8} f \quad (m^{-1}) \quad \text{(D-5)}$$

and therefore the condition

$$|\gamma_0 \rho| = |2.096 \times 10^{-8} f \rho| << 1 \quad \text{(D-6)}$$

is satisfied easily for the frequencies f and ranges ρ of interest.

Condition 2. $|\gamma_1 \rho| >> 1$

For frequencies of interest, it can be shown that the first term on the right side of equation (D-1) is many orders of magnitude smaller than the second term and, therefore, negligible in comparison. Thus, the modulus

$$|\gamma_1| = (\omega \mu \sigma)^{1/2} = (2 \pi f \mu_0 \sigma)^{1/2} = 5.620 \times 10^{-3} f^{1/2} \quad (m^{-1}) \quad \text{or} \quad \text{(D-7)}$$

$$5.620 \times 10^{-3} f^{1/2} \rho >> 1. \quad \text{(D-8)}$$

It follows that the horizontal component of range ρ must therefore satisfy the condition

$$\rho >> 177.9/f^{1/2} \quad (m). \quad \text{(D-9)}$$

If the symbol ">>" is interpreted as meaning "ten times greater" then the range ρ must exceed $1779/f^{1/2}$. Thus, for f = 1 Hz, ρ must exceed 1779 m and, for f = 4 Hz, ρ must exceed 890 m.

Condition 3. $\rho >> |h|$

If, for example, the depth of the HED is 100 m, the equations are valid for ranges ρ greater than 1000 m, if the above interpretation of ">>" is held.

Condition 4. $\rho >> |z|$

If the above interpretation of ">>" is held, the equations are valid only if the horizontal component of range ρ of the underwater field point P exceeds ten times the depth of P; i.e., only if the angle subtended at a point on the surface directly above the HED between the sea surface and point P is less than 5.7° (i.e., arctan 0.1). Thus the equations of figure D-1 cannot be validly applied to the full hemisphere below the HED.

Subject to the above six conditions, the equations of figure D-1 can be recast to yield the magnetic induction at field point P in a manner similar to that used in Appendix C as follows.

Case I. $z \leq 0$ (P in seawater)

$$B_{\rho 1} = [400\, p_s \sin\phi / (\gamma_1 \rho^3)]\, \{\exp[\gamma_1 (h + z)]\} \tag{D-10}$$

$$B_{\phi 1} = [-200\, p_s \cos\phi / (\gamma_1 \rho^3)]\, \{\exp[\gamma_1 (h + z)]\} \tag{D-11}$$

$$B_{z1} = [600\, p_s \sin\phi / (\gamma_1^2 \rho^4)]\, \{\exp[\gamma_1 (h + z)]\} \tag{D-12}$$

Case II. $z \geq 0$ (P in air)

$$B_{\rho 2} = [200\, p_s \sin\phi / (\gamma_1 R^3)]\, [\exp(\gamma_1 h)]\, [2 - (3 z^2 / R^2)] \tag{D-13}$$

$$B_{\phi 2} = [-200\, p_s \cos\phi / (\gamma_1 R^3)]\, [\exp(\gamma_1 h)] \tag{D-14}$$

$$B_{z2} = [600\, p_s \sin\phi / (\gamma_1^2 R^5)]\, [\rho \exp(\gamma_1 h)]\, [1 + \gamma_1 z - (5 z^2 / R^2)] \tag{D-15}$$

Case III. $z = 0$ and $h = 0$ (Both field point P and HED at air-water interface)

$$B_\rho = 400\, p_s \sin\phi / (\gamma_1 \rho^3) \tag{D-16}$$

$$B_\phi = -200\, p_s \cos\phi / (\gamma_1 \rho^3) \tag{D-17}$$

$$B_z = 600\, p_s \sin\phi / (\gamma_1^2 \rho^4) \tag{D-18}$$

Equations (C-11), (C-12), and (C-13) can be used with the preceding nine equations to determine the magnetic anomaly produced in the earth's field in each of the above three cases.